
Algebraic model for negative focused ultrasound beam width

- By Christian Elmholt Jakobsen-

Project Report
16gr10406

Aalborg University
Health science and technology



Health science and technology

Aalborg University

<http://www.aau.dk>

AALBORG UNIVERSITY
STUDENT REPORT

Title:

Algebraic model for negative focused ultrasound beam width

Theme:

Ultrasound imaging

Project Period:

Spring Semester 2016

Project Group:

16gr10406

Participant(s):

Christian Elmholt Jakobsen

Supervisor(s):

Samuel Schmidt

Alex Skovbo Jørgensen

Martin Vandborg Andersen

Copies: 0

Page Numbers: 64

Date of Completion:

May 31, 2016

Abstract:

Conventionally ultrasound uses unfocused and focused beams to gather image information in tissue. However limitation in the acquisition speed has been reached and new techniques need to be developed to overcome these. Negative focus has in few cases shown potential to solve this by providing a wider beam thus enhancing the parallel focusing capability in ultrasound. There is however still a lack of knowledge for the negative focus compared to the unfocused and focused beam. This project has determined an algebraic model bringing together the influential factors aperture size, negative focal distance and range to determine the beam width. The model was validated with good results and shows how the beam width is a projection of the aperture. This model is based on a newly developed technique to simulate ultrasound beams and validated with measurements of the beam width from two transducers. The model has the potential to combine the separate theories of the three beams into one.

The content of this report is freely available, but publication (with reference) may only be pursued due to agreement with the author.

Contents

Preface	ix
1 Introduction	1
1.1 Initial Problem	2
2 Problem analysis	3
2.1 Ultrasound Imaging	3
2.2 Coherent Pulse	7
2.3 Transmit and Receive Response	9
2.4 Image Resolution	11
2.5 The unfocused beam	12
2.6 Focused and negative focused beams	14
2.7 Problem statement	18
3 Problem Solution and Model determination	19
3.1 Method	19
3.2 Simulation of beam width	20
3.3 Algebraic Model Estimation	24
3.4 Experimental protocol	30
3.4.1 Procedure	30
4 Results	33
5 Discussion	43
6 Conclusion	47
Bibliography	49
A Equipment	51
A.0.1 Hydrophone	51
A.0.2 Oscilloscope	51

A.0.3	VMI transducer	51
A.0.4	HPS 12 transducer	51
B	Hydrophone datasheet	53
C	Model formulation	57
C.1	Conceptualization	57
C.1.1	Coherent Pulse	58
C.1.2	Time delay	59
C.1.3	Attenuation	59
C.2	Attenuation due to frequency	60
C.2.1	Dissipation of the pulse (Attenuation due to range)	60
C.2.2	Directivity function (Attenuation due to angle)	61
C.3	Realization	61
C.3.1	Maximum Peak Amplitude - Mapping	62

Todo list

Preface

This project is sequel to the project "Generic Ultrasound transducer simulation" which can be found in the AAU database, it is recommended to read the prequel before this project, but not necessary. This Project is for experience engineers and others with interest in ultrasound imaging.

Aalborg University, May 31, 2016

Christian Elmholt Jakobsen
<Ceja11@student.aau.dk>

Chapter 1

Introduction

In many fields of medicine it is beneficial to assess anatomical structures without having to resort to surgical manipulation. Ultrasound imaging does this in a cheap and reliable way and has become a common practice in cardiology. Ultrasound imaging in cardiology is used to determine structural problems in the heart such as valves insufficiency and cardiac effusions. The ultrasound image is created by emitting sound pulses into tissue and recording the echo. The ultrasound pulses travels from the transducer into the tissue where it encounters layers of different tissue with changing density. The tissue layers reflects some of the pulse back to the transducer where it is measured to create the image.

one of the limitations of ultrasound is the velocity of sound this limits the acquisition rate which is determined by the time it takes to transmit and receive. [1]. This means the number of transmit and receive (Tx, Rx) cycles is fixed and cannot be increased. Thus it is important to optimize every Tx and Rx cycle to acquire as much image information as possible, to gain resolution and frame rate. To increase the amount of information pr. Tx and Rx cycles, a technique call "Parallel focusing" can be applied. Parallel focusing is when the beam is intentionally widened, this results in reflections from a larger area of the field of view (FOV). The FOV is the area of which all the data for an image is gathered. The structural image information from each location is then extracted with computer processing afterwards this functions as source separation since the beam is not localized anymore.[7].

The increased frame rate or resolution could potentially benefit the diagnostics but could also unveil new information to diagnose other conditions. One way to widen the beam is to use a negative focus. The negative focus has only been used in very few cases to create actual images and has been shown to help design High frame rate electrocardiography [5]. The negative focus is a technique to shape the beam, spreading out the pulse. There is no known way to easily calculate the beam width of a negative focus beam besides doing simulations until a desired beam width is found by trial and error. Therefore an algebraic model to determine the beam

width for desired settings would be beneficial.

1.1 Initial Problem

What knowledge must be considered to adequately estimate parameters for a certain beam width transmit response using negative focus?

Chapter 2

Problem analysis

In this chapter a description of the general principles of ultrasound imaging is presented. The physics behind the acoustic wave will be described and how the different plots and graphs is calculated to simulated these phenomenons. Different beam types will also be investigated and the knowledge is used to predict beam characteristics. This information is important in order to understand the problems and assumptions used in ultrasound imaging. The mathematical descriptions used in the imaging is therefore essential knowledge to find the parameters for the best estimate of the negative focus and circumventing the limitation of ultrasound e.g. the limited speed of Tx and Rx cycles.

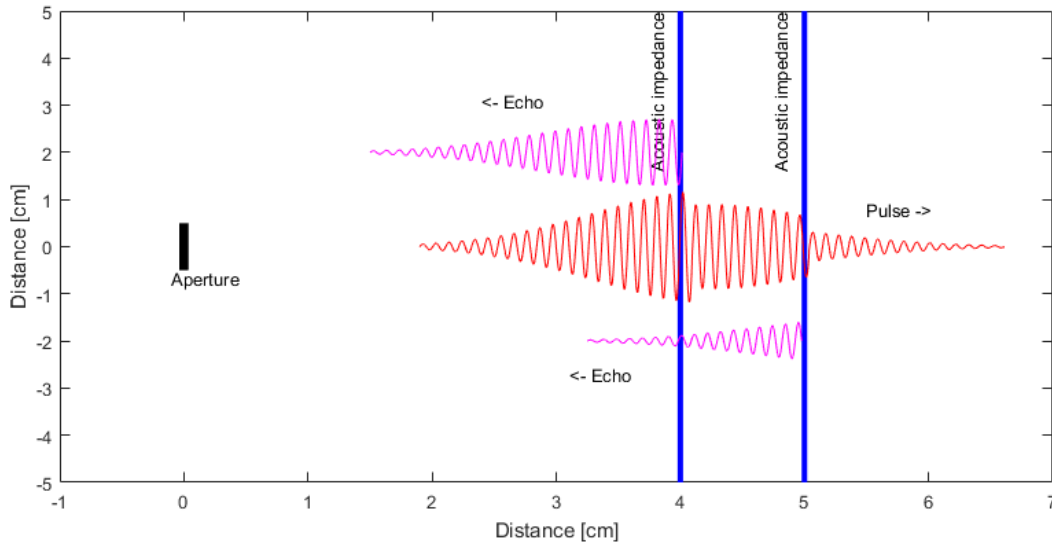
2.1 Ultrasound Imaging

In order to estimate the which parameter that is important to shape the ultrasound beam a basic understanding of the imaging technique must be obtained. The components of the transducer and the origins of the pulse will be described. The basic of how the ultrasound image is created will also be described.

Ultrasound is defined as the sound frequency higher than the human ear can perceive, meaning 20kHz or higher. In ultrasound imaging a frequency of 2-10 Mhz is conventionally used. Ultrasound imaging uses sound pulses emitted into tissue which create a measurable echo from changes in density or elasticity, also known as changes in acoustic impedance. As the pulse propagate through the layers of different tissue, different acoustic impedance is encountered. Some of the acoustic energy in the pulses is reflected, some is scattered or absorbed the remainder of the energy continues through ensuring a echo each time the acoustic impedance changes see Figure 2.1.

The reflected pulses is then measured and used to create the image. The average speed of sound in human tissue is 1540 m/s. The velocity of the pulse is

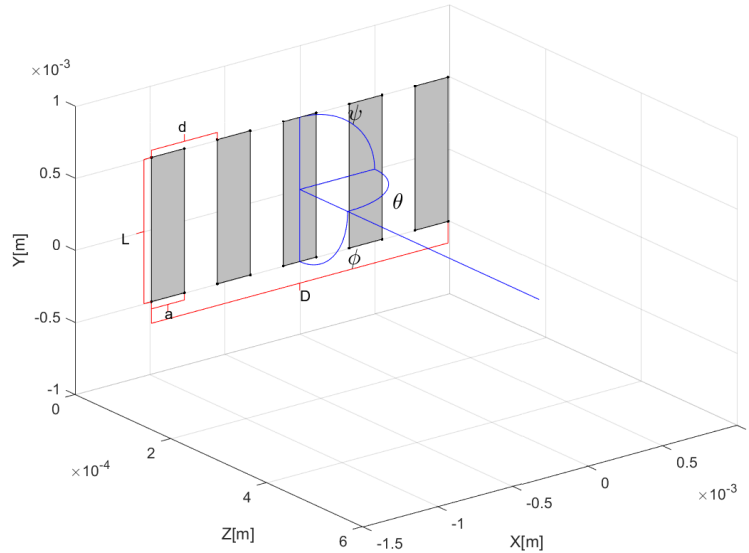
Figure 2.1: Illustration of how the reflections are generated. The blue vertical lines are acoustic impedances. The red sinus is the pulse emitted from the transducer. The magenta sinuses is the reflected pulses.



changing based on the small changes in acoustic impedance. The average speed is used instead of the impractical approach of the constantly changing speed in tissue as it propagate. The speed of sound in tissue means that there is a ceiling to how many Tx-Rx cycles before e.g. the heart has change shape by contracting thus the image must be created fast to avoid motion artifacts. When the ceiling is reached the only way to increase resolution or frame rate would be to increase amount of image information pr cycle.[2] These high frequency pulses are made by applying a electrical charge to a piezoelectric element converting the electric energy to pressure waves (sound waves). This phenomenon, known as the piezoelectric effect, works in reverse and can convert the returning echo of sound waves to an electric signal. This electrical signal can be sampled and the amplitude represents the acoustic impedance of medium interface reflecting it. The location of the interface which provided the echo is calculated with the averages speed of the pulse and the time to travel back and forth to the interface location. Ultrasound transducers have multiple piezoelectric element the elements are placed in a line or grid call an array see Figure 2.2.

The elements can be timed to emit pulses with different timings, which is known as phased arrays. The timing of the pulses, known as the delay function, makes them add together in some area creating a wave front which is sum of each elements pulse in their respective phase. This is done in order to maximize the echo making it more detectable. The sum of multiple pulses in a single spatial

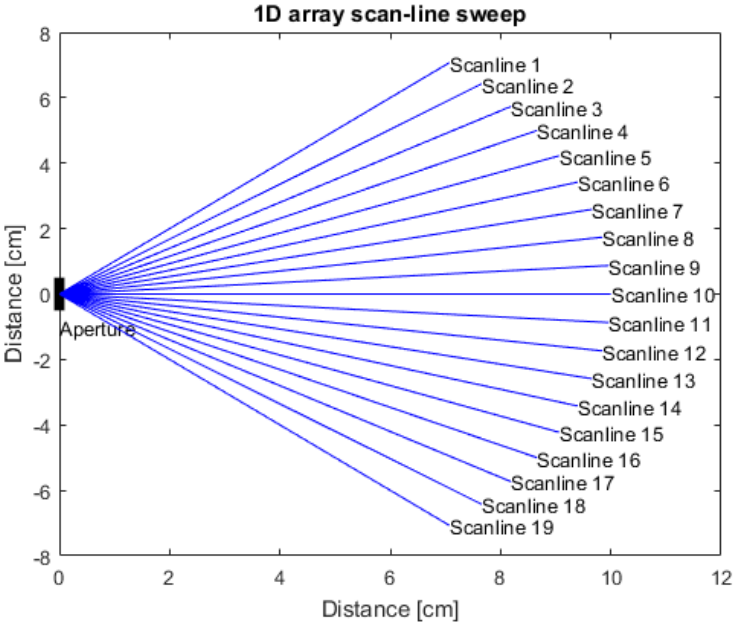
Figure 2.2: Array setup in a transducer with rectangular elements, Only five elements are shown for simplicity. a is element width, L is element height, d is the distance between elements, θ is the azimuth angle and ϕ is the elevation angle ψ is the rotational angle.[4]



location is call a coherent pulse. The coherent pulse has a larger amplitude than the individual pulses thus creating a larger echo. All spacial locations where the coherent pulse can generate a detectable echo is known as the beam and this can have several different shapes and characteristics. The beam is usually emitted to scan a single line in the FOV, this is known as a scan-line. The scan lines is angled differently in the next Tx-Rx cycle, effectively sweeping the FOV for image information, see Figure 2.3. The echo recorded from each element is the superposition of echoes from multiple locations, with same the distance from that element. However with multiple element it is possible to sort out the original echo source by taking the delay between each element into account this is also how the source separation in parallel focusing works.

The combined width of the array elements is the aperture. The aperture is limited by the way it is used for medical imaging it has to fit between the ribs or down the throat for transesophageal echocardiograph which gives a maximum aperture of 2cm. The aperture size limits the resolution and energy due to the Rayleigh criterion, which will be explained later in section 2.4, and the limitation of energy, set by law, that tissue can be exposed to. [7]

Figure 2.3: Illustration of image data acquisition scanning line by line, starting at scanline 1 down to scanline 19.



2.2 Coherent Pulse

Calculating the coherent pulse is one way to gain insights to different beams. This section describe how the coherent pulse is calculated and later it will be shown how multiple of these calculation can estimate the Tx response which is necessary to estimate the beam width for any type of beam. This is one way to gain insight to how the negative focused beam width is influenced.

The aperture of a ultrasound transducer consist of an array of piezoelectric elements. Each element can emit acoustic pulses by electric stimulus through the elements. The summation of these pulses is the coherent pulse. The coherent pulse differs with varying spacial location as the pulses add up in different phases. Depending on the distance from their individual origin and angles to the apertures normal vector the coherent pulse will end up with different length and amplitude. The pulses are also attenuated as a function of distance and frequency[2].

$$U_z(t) = \sum_N^{i=1} U(t - \frac{d_i}{c} + t_i) \cdot A_f(f, d_i) \cdot A_d(d_i) \cdot A_\theta(\theta_i, \phi_i) \quad (2.1)$$

Formula 2.1 is used for calculating the coherent pulse, multiple of these are used to simulated the beam this technique is derived and used in previous work[4] a more detailed description of the calculations can be found in Appendix C.

Where $A_d(d_i)$ is distance dependent attenuation a result of the spherical expansion of the wave, dissipating the pulse energy. When the acoustic energy is spread out over a larger area as it propagates form the source. The result is an attenuation which resembles decay in an $1/r$ fashion.

The frequency dependent attenuation ($A_f(f, d_i)$) is an exponential loss, due to absorption and scattering of the acoustic energy as the pulse propagates. This attenuation also depends on the distance from the transducer, also known as the range, and the medium and frequency. The material constant α defines this loss, but can be neglected in some materials such as water due to its low impact on results see table 2.1 [2]. As an example the frequency dependent attenuation of a 5MHz pulse at 10cm range in water would be $0.002 \cdot 10cm \cdot 5MHz = 0.1dB$ which corresponds to a loss of 1.14 % acoustic energy due the waters converting the wave to heat.

$A_\theta(\theta_i, \phi_i)$ is the angle dependent attenuation and is a result of the directivity of the individual element in the array. The attenuation is a result of a element interfering with it self. [10]. The angle dependent attenuation ($A_\theta(\theta_i, \phi_i)$) is derived with Huygens Princip which stats

"Every source of waves which α is much less than λ may be considered as a source of a spherical wave[2]."

This means all pulses that does not propagate in the direction of the normal to the individual element is attenuated due to the interference with itself. Using this it is possible for element of any geometric shape to calculate its directivity function with the assumption that it can be divided into segment infinitesimally small that all act as a spherical source[2].

These three attenuations are used to estimate each pulse at a specific location and shift according to their individual arrival and add together to obtain the coherent pulse. $U(t - \frac{d_i}{c} + t_i)$ is the pulse at origin and $U_z(t)$ is the coherent pulse. f is the center frequency of the pulse, d_i is the distance from the i 'th element, θ_i is the azimuth angle for the i 'th element, ϕ_i is the elevation angle for the i 'th element and t_i is the delay time for the i 'th element [4].

Table 2.1: Table for alpha values in different materials [2]

Material	α [dB/(cm MHz)]
Water:	0.002
Blood:	0.15
Fat	0.6
Liver	0.9
Kidney	1
Brain	0.8

It has been shown how to calculated the coherent pulse, an estimate of the combined acoustic energy output from a transducer at a single spacial location. This is a key tool for to simulate the beam and understanding its properties.

2.3 Transmit and Receive Response

The Tx response is used to estimate the characteristic of the transmitted ultrasound beam at a selected range. The Rx response is how the echoes are received and added together. The beam width can be estimated from the Tx response in several ways however, only one way will be described and used in this section.

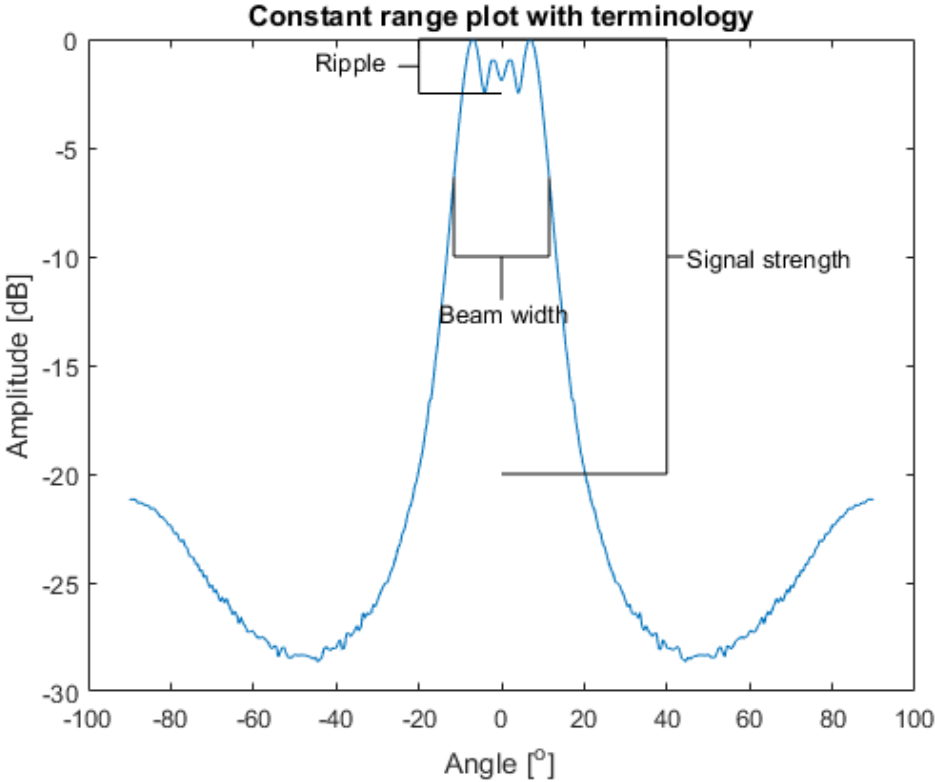
The beam illustrates the distribution of the acoustic energy in the FOV, it is created from the maximum values of coherent pulses. The Tx response is also the distribution of acoustic energy at a selected range, it can be considered a single slice of the beam. The spatial location where there is constructive interference will make the Tx response peak. More acoustic energy will result in larger reflection which is easier detectable for the transducer. The Tx Response is also known as a constant range plot (CRP) see Figure 2.4. There are three characteristics noticeable in the Tx response: the ripple, the signal strength, and the beam width. The characteristics of the Tx response change with different transducers. If the transducer does not have enough signal strength, the reflection will not generate a detectable signal and the image will be black. If the ripple is too large, the amplitude of the reflections will be distorted and the image will be unreadable. The Rx response is how the sampled signal is shifted in time and added together to create the image data. The shift is usually done in a focused manner such that reflections from a certain angle and range will add together and reflections from other spatial locations will not, leaving a spatially localized measurement. The Rx response amplitude depicts the sensitivity of the transducer. [7].

To estimate Tx response, the $U_z(t)$ is calculated using Formula 2.1 for each spatial location in a selected area. The maximum value of each coherent pulse is used as the Tx response amplitude. For a Tx response, this area is only at a chosen range and the coherent pulse is then calculated for all angles from -90° to 90° with a selected step size. In the Tx response, the beam width can be found as where the Tx response has attenuated -6dB from its own maximum. Linear extrapolation can be used to get a more accurate result between data points. The same goes for the Rx response; however, only a focused beam is used for the Rx response. The Rx and Tx responses are also known as constant-range-plots. [4].

The Tx and Rx response can be multiplied to find the overall system response which gives a good estimate of the resolution for a given aperture. It is important that the overall system response still can provide adequate resolution as a wide Tx response has the opposite effect. If it does not provide adequate resolution, a more narrow Tx response must be chosen. With a wide enough Tx response, multiple Rx responses may be used [7].

It has now been shown how to simulate the Tx response and extract the -6dB beam width for any beam at any range. This knowledge can be used to estimate

Figure 2.4: An example of the transmit response of an unfocused array. The ripple, signal strength and beamwidth is shown



how different variable might influence the beam width or other characteristic of the beam.

2.4 Image Resolution

Some of the physical phenomenon occurring in the aperture limits the resolution of the image. This means there is maximum resolution for each different transducer, trying to obtain better resolution will waste the resources such as Tx-Rx cycles and it is therefore important to understand and take into account.

To create a picture from ultrasound waves it is important to understand the limits of the waves as they diffract through an aperture. The diffraction through an aperture result in blurring of the image which means a certain aperture has a maximum resolution. Angular resolution is the angle which objects smaller than that angle cannot be resolved. The resolution is determined by the Rayleigh's criterion. In other terms this limit is use to calculate the minimum angle between two sources in order to tell them apart. Without changing the diameter of the aperture or the frequency and subsequently the wavelength the resolution cannot be increased. The angle does depend on the shape of the aperture and for a circular aperture the diffraction limit (θ_c) can be determined by Equation 2.2 and for a square aperture the diffraction limit (θ_s) by Equation 2.3 [3]. This diffraction limits determine the amount of scan lines from the optimal resolution given the FOV. e.g. if the diffraction limit is 2° and the FOV is 90° , 45 scanlines is need to optimally cover the FOV for 1D arrays. The number of scanlines can increase dramatic when using 2D arrays. The same example in 2D would require $45 \cdot 45 = 2025$ scanlines. 2025 scanlines at a range of 15cm would results in a maximum of $1540 / (2 * 0.15) = 5133$ scanlines pr. second and with 2025 scanlines pr frame results in 2.54 frames pr. second. This number can however be increased by using parallel focusing, effectively scanning more than one line pr. Tx-Rx cycle but result in more post processing to sort out the information in each line.

$$\sin(\theta_c) = 1.22 \cdot \frac{\lambda}{D} \quad (2.2)$$

$$\sin(\theta_s) = \frac{\lambda}{D} \quad (2.3)$$

θ_c is the minimum angle between to sources to tell them apart for a circular aperture. θ_s is the minimum angle between to sources to tell them apart for a square aperture. λ is the wavelength. D is the diameter of the aperture. The resolution in range is determine by the pulse length and is simply half the pulselength.

This section have shown where the physical limitations of ultrasound image is set and what variables that influence these limits. It is important to take into account to avoid wasting resources. It is also seen that the wavelength and the aperture size is very influential variables.

2.5 The unfocused beam

To estimate a model of a beam can prove very difficult indeed if the model cannot be any formula approximation, such a high degree polynomial. It would be beneficial to know how the characteristics of known beams behave to determine if any similarity exist to hypothesize how a simple model could be determined.

The beam can change shape based on how the elements in the array are fired, the delay between each element can usually be determine with a function, known as the time delay function. An unfocused aperture is where all elements are fired simultaneously, the delay function is 0, no delay between any elements. For any aperture there is certain fields or distances from the transducer where the nature of the beam changes character. For an unfocused aperture these are called the near field and the far field. The near field is more influenced by interference which is seen as the ripple, than in the far field where the beam is less fluctuating[7]. The transition from near to far field (Z_{far}) is determine by the last on axis maximum and is given by Formula 2.4 see Figure 2.5 The on axis direction is the direction that the transducer is pointing same directions as the normal vector of the array.

$$Z_{far} = \frac{D^2}{4\lambda} = \frac{D^2 \cdot f}{4 \cdot c} \quad (2.4)$$

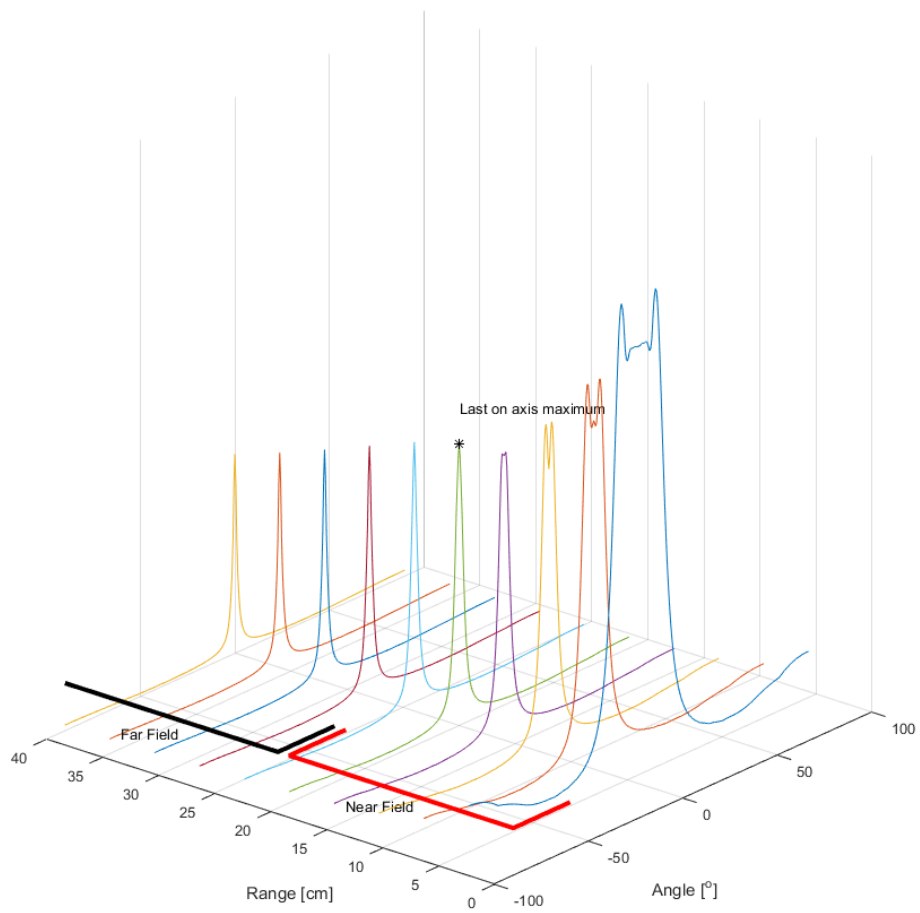
In the far field the beam is cone shaped. The angle of the cone is known as the beam spread and can for a unfocused aperture be determine with formula 2.5. The beam is wider in the near field and after the last on axis maximum it approaches the beam spread angle asymptotic.

$$\sin(\theta_{far}) = 1.2 \frac{c}{D \cdot f} = 1.2 \frac{\lambda}{D} \quad (2.5)$$

θ_{far} is the half angle of the 6dB beam spread in the far field.

It has been shown that the unfocused beam has certain zones and points of interests which can be mathematical described, both of which can be determine from the wavelength and aperture size.

Figure 2.5: Illustration of the near field and the far field in an unfocused beam, the last on axis maximum is marked with * and is where the beam change from the near field to the far field. Notice the lack of ripple in the far field.



2.6 Focused and negative focused beams

In this section the focused beam and some of the focusing techniques will be described. The negative focus is a special case of the focused beam it is expected to have some similarity to the focused beam and give some insight towards how a potential model of the negative focused beam could look.

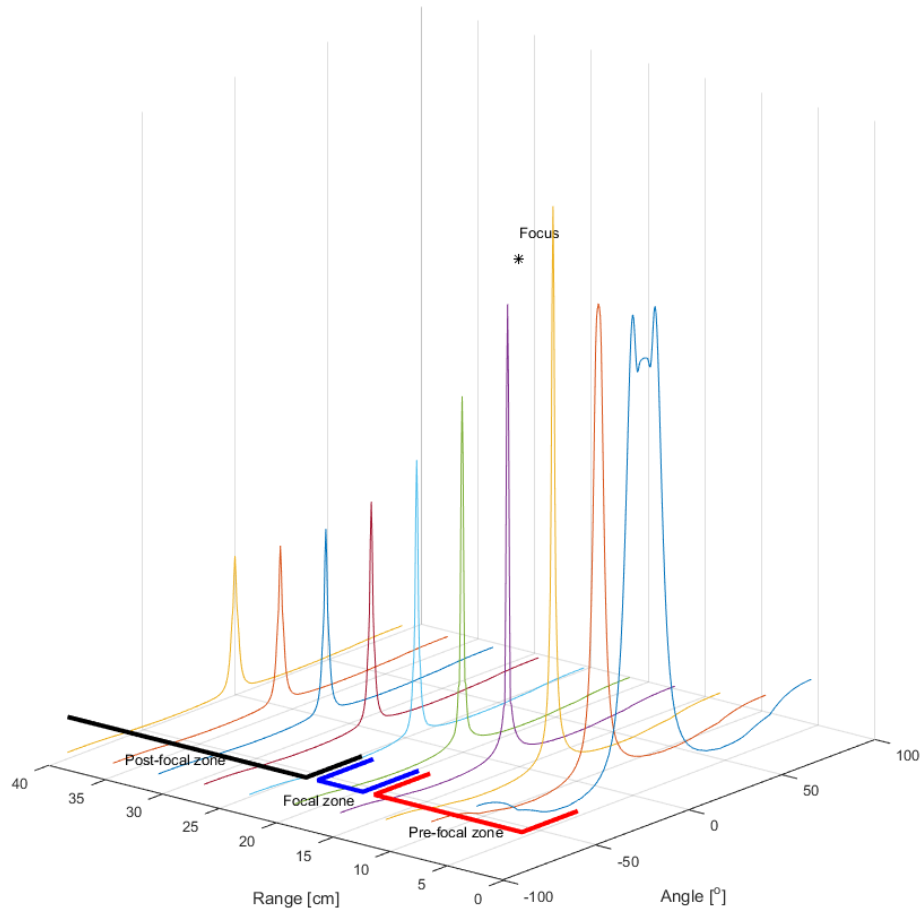
To focus a beam all elements are timed to fire so that the pulses meet at one spacial location at the exact same time. This spacial location becomes a very narrow beam with very high amplitude at the focus location making it easier to detect. When using focused arrays the notation of near and far field makes less sens as it does not fit convictions. The terms postfocal, prefocal and focal distance is used. The focal field, also known as the focal Fraunhofer zone, is where the array is focused. Postfocal, also known as the far Fresnel zone is from the focal Fraunhofer zone and beyond. The prefocal, also known as the near Fresnel zone, is everything from the aperture to the focal Fraunhofer zone. [7]. See Figure 2.6.

In order to optimized image information pr Tx-Rx cycles parallel and dynamic focusing can be used. This is possible because the post receive processing which allows multiple Rx responses. Parallel focusing uses multiply angles for the Rx response delay function. For a simple example if the Tx response is 30 degrees wide and the Rx response is 6 degrees wide 5 lines can be scanned with one Tx-Rx cycle See figure 2.7. Since each Rx response separates the information from the different spacial locations covered by the beam. Each Rx response has a unique delay function the recorded signal from each element is delay according to its respective Rx response and then added together. Since this process is done afterwards and independent of the Tx-Rx cycle it can be done multiple times. The dynamic focusing uses different focus distances and can be applied in the same fashion as parallel focusing. by applying both focusing techniques the entire beam area can be separated in spacial localized measurement derived by processing of the measured data. The Rx response is best used as narrow as possible. This makes it the easiest to distinguish different objects but cannot increase the resolution above the Rayleigh criterion. [7]

The aperture has a natural focus distance given by Equation 2.4. It is possible to change the focus distance with the delay function. However the natural focus distance and the applied focus distance (F) has a reciprocal relationship. The combined focus is (Z_{far2}) can be calculated using Equation 2.6. [7]

$$\frac{1}{Z_{far2}} = \frac{1}{Z_{far}} + \frac{1}{F} \quad (2.6)$$

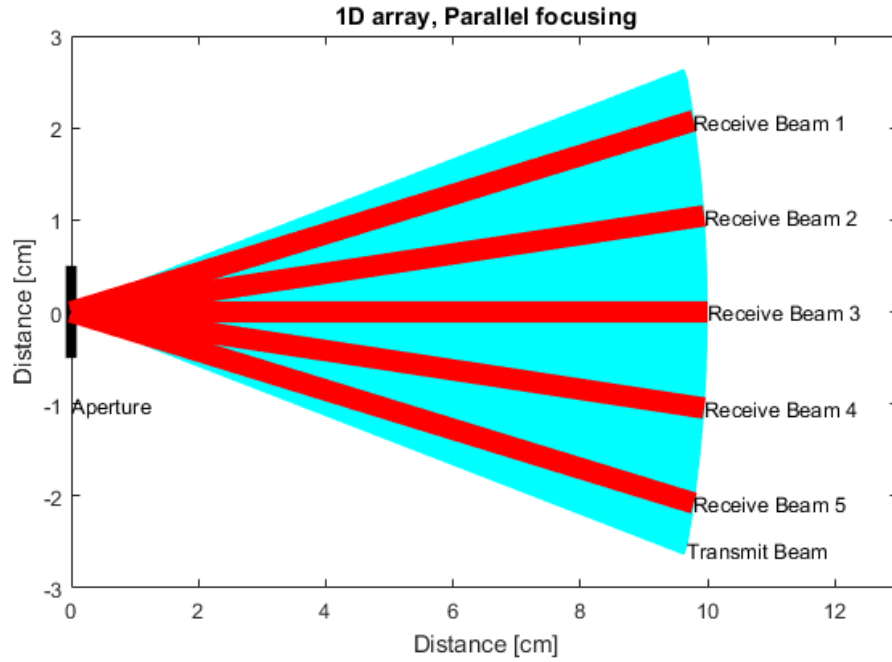
Figure 2.6: Illustration of the zones in a focused beam. Notice the high amplitude near the focus and the extremely narrow beam.



Z_{far2} is the resulting focus distance from the aperture

In the focused beam there is a relation between the number of wavelengths for a beam width (\hat{x}_{-6dB}) and the aperture (\hat{D}) and range in wavelength (\hat{z}) for the far Fresnel zone se Equation 2.7[7]. It is possible that a similar relationship exist for the negative focus as well.

Figure 2.7: Illustration of parallel focusing where 5 receive beam is fitted within one transmit beam



$$\hat{x}_{-6dB} = \frac{b \cdot \hat{z}}{\hat{D}} \quad (2.7)$$

Negative focus are only used to create the Tx response. The same formula for calculating the delay function (Δt_n) is used as for the normal focus see Equation 2.8. However the focal distance is negative. A negative focus close to the transducer will provide a wider beam than one further away as the beam tends to diverges more then other beam types.

There is no known categorization of the zones or distances for the negatively focused beam which leaves the determination of the beam width with a problem as there is no know point of reference to obtain similarity for the transmit response contrary to the unfocused.

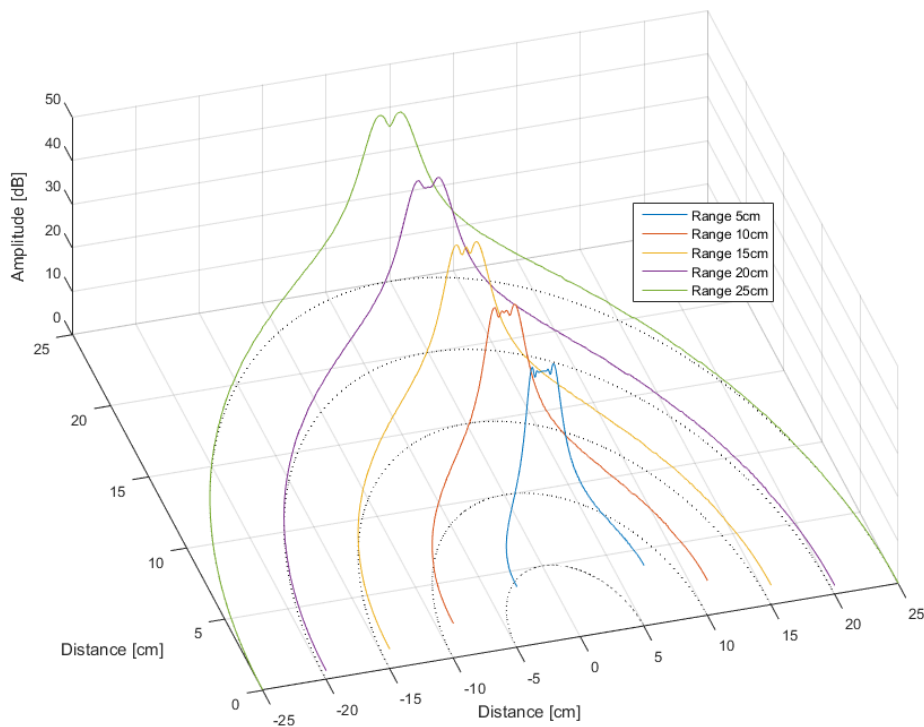
It is unknown how to obtain a desired beam width with the negative focus other then trail and error. The negative focus has proven useful in creating High frame rate echocardiography[5]. A model to better assess the beam width would be beneficial.

$$\Delta t_n = \frac{F}{c} \left(1 - \left[1 + \left(\frac{nd}{F} \right)^2 - \frac{2nd}{F} \sin\theta \right]^{\frac{1}{2}} \right) + t_0 \quad (2.8)$$

Where Δt_n is the delay function to achieve a focus at distances F with n elements d distance apart in a medium with speed c at an angle of θ . t_0 is a offset to avoid negative delays. [9]

The negative focused beam is illustrated in Figure 2.8 which visualize the transmit response at different ranges. What is also seen in the center of the beam is the ripple which fluctuate close to the aperture, less further away and completely vanish very far away, this also depends on the focal length and the aperture size see Figure 2.8 .

Figure 2.8: Simulation of the transmit response at different ranges. 21.1mm array, 101 element $\lambda x \lambda$, 3.5Mhz, focus -28cm



2.7 Problem statement

From the analysis it is seen that there is no known way to calculate a desired width for a negative focused beam. There is a lack of information about the negative focused ultrasound beam in general, and the negative focused beam could be useful in parallel focusing due to its changing width with different negative focus distance.

It has been shown that the focused beam can be determined from the far field from the range and the aperture size and a constant which need to be found numerically. The overall influential variables seem to be aperture size and the wavelength, however the focal distance plays a significant role for the adaptability of the negative focused beam. This variable should be investigated further and if the beam width can be adjusted to any size only changing the focus any existing transducer could benefit from this model. Since it is easier to change the focus than the aperture size. It is also shown that the focused beam does provide a formula for the far Fresnel zone which has a similar effect as the negative focused beam and might create a great starting point for the search of an algebraic model of the negatively focused beam width.

The mathematical descriptions previously mentioned can help determine the characteristics of focus and unfocused beams and the variables aperture size and focal distance seem to be the most influential on the focused beam. Therefore there might be a similar relationship for the negative focused beam. This leads to the question:

How does the aperture size and focal distance influence the beam width of a negatively focused beam?

Chapter 3

Problem Solution and Model determination

In this chapter it will be shown how the simulations is done. The simulations will be done with the new technique developed in previous work to avoid making large amount of beam width measurements. Further more the simulation will shed some light on the expected relations between the variables, aperture size and focal distance for one-dimensionally arrays. Here after an algebraic model will be created and validated with measured data.

3.1 Method

To establish the foundation of an algebraic model a large number of simulation will be conducted. This is done instead of doing multiple measurement with several different array sizes which would be impractical due to the number of transducers available. The independent variables, Focal distance and aperture size, will be evaluated over an interval and the dependent variable, beam width, will be calculated for each unique set of variables. This will provide the data for a curve fitting which will optimize an unconstrained constants in the function evaluated by a goodness of fit test. The function which the data will be fitted to will be derived from each independent variable relationship with the beam width.

3.2 Simulation of beam width

The simulations is done with a technique developed in previous work a more detailed description of the calculation can be found in Appendix C. The simulations of the beam width is done to adequately estimate the model. The simulation are used instead of measuring a large amount of beam widths which would be extremely time consuming and would provide very little coverage of the aperture sizes, the simulations can provide all sizes of the aperture. Afterwards the model needs to be validated with new measurements of the beam. The simulations was validated in the previous work [4] and can adequately depict the beam characteristics. However a correlation between measurement and simulated data with same setting for the negative focus will also be used to validate the results.

The simulations is accomplished by estimating the coherent pulse at selected location along an 180° arc see Figure 3.2. The maximum peak value of the coherent pulse is used as data points for a CRP see Figure 3.1. The reference value, in the CRP, is the value consider 0 dB and is the chosen to be the maximum peak in the CRP. It is in the CRP the beam width the information can be found. The -6dB angle is found by linear extrapolation between the two closest data point to get more accurate beam width. This leaves an isosceles triangle where the unique angle, is the beam width angle, and length of the two identical sides each are the range, the unknown side of the triangle is the beam width which can be calculated geometrically see Figure 3.2.

To examine how the beam width changes with aperture size and focal distance each independent variable is simulated with different values while the other is kept constant, The parameter for all simulations is seen Table 3.1. This is done multiple times only changing one variable and then plotted as seen in Figure 3.3 where aperture size is change and 3.4 where the focal distance is change. It is seen there is a reciprocal and linear relationship between the variables and the beam width, which can be used to determine a combine function

The element size, for the simulations, was chosen to be $\lambda \times \lambda$ as this ensure a spherical directivity function and thus making the element any smaller would not influence the beam width in any way. The directivity of the elements determines in what direction the elements acoustic energy is emitted. A larger element will have a narrow width thus limiting the beam spread and an element smaller than the wavelength distribute the energy uniformly also known as spherical according to Huygens principle. The beam width estimation does not take into account the ripple in the beam, which could be more than 6dB making the beam split in two. This only happens with very short negative focus distance or very wide arrays, approximately when $F < D/2$. Neither does it take the signal strength in consid-

Figure 3.1: Simulated CRP. Range: 7cm, Aperture: 2cm, Focal distance: -10cm, Pulse frequency: 3MHz, 1D-array, 100 element. elements is a $\lambda \times \lambda$ square. The Beam width angle is 27° ($2 \times 13.5^\circ$) and at a 7cm range it results in a beam width of 3.27cm

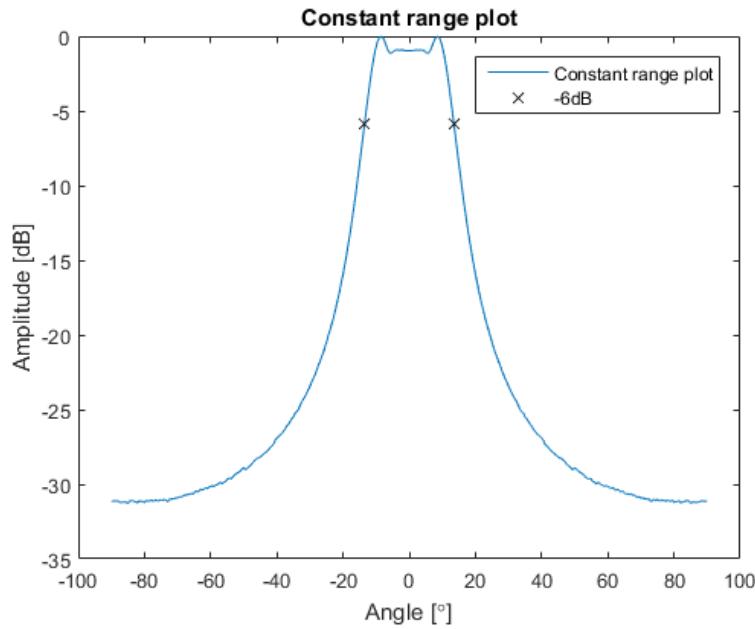
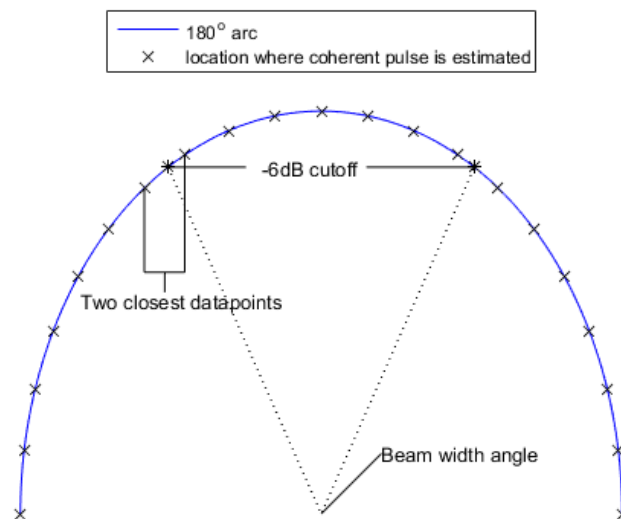


Figure 3.2: Illustration of how the -6dB cutoff is found and subsequently how the beam width is found geometrically. The distance between the two -6dB cutoff is the beam width



eration. 3MHz was chosen as the frequency since it is a common used frequency that allow the acoustic penetration and still provide adequate resolution. The range chosen for the simulations was 7cm= 140λ since no other point of reference could be deduced from the physics such as in the unfocused or focused case with the natural focus. The 7cm is the approximately range to image the center of the heart and commonly used in transducer validation. The alpha value was chosen to be 0 since the measurements is done in water where the frequency dependent attenuation can be neglected.

Through the work of estimating the algebraic model multiple stages of simulations has been done they are summarized here:

1. Simulations only changing one variable to determine its relationship to the beamwidth.
2. Simulations change both variables to create a large data set to fit and test the algebraic model.
3. Simulation of similar settings as the measurements to compare with the measured data.

Table 3.1: The parameters used for each simulation. N is the number of elements

Sim	Element size	N	f (MHz)	Z	F	D
1.	$\lambda x \lambda$	100	3	7cm	-1 to -30 cm	0.5 to 3cm
2.	$\lambda x \lambda$	100	3	5-10cm	-3 to -30 cm	1 to 2.5cm
3.	14x0.22, 7x0.1 (mm)	96	3.57, 7.14	7 and 10cm	-10 and -20cm	21 and 9.6mm

Figure 3.3: Beam width Vs. Aperture width plot. Range: 7cm, Pulse frequency: 3MHz, 1D-array, 100 element. elements size $\lambda \times \lambda$ square

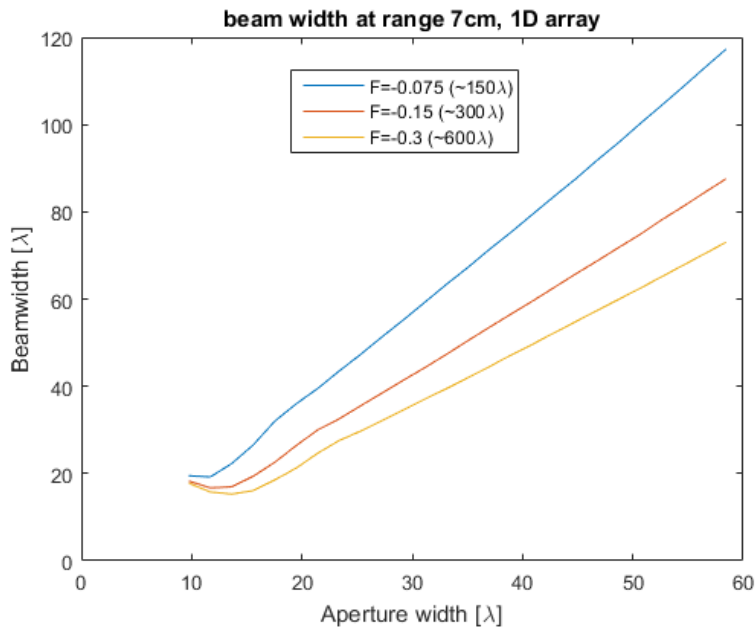
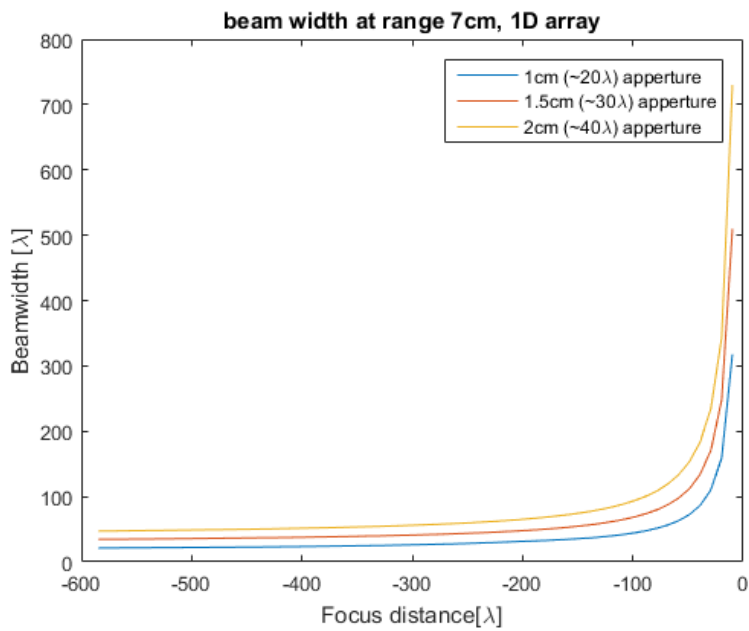


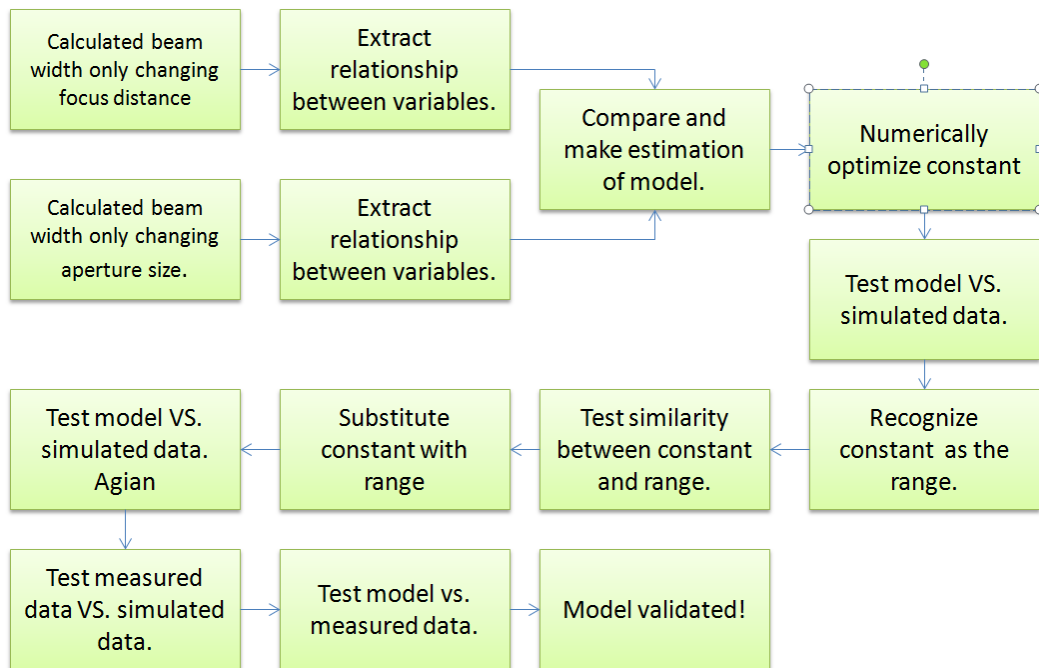
Figure 3.4: Beam width Vs. Focal distance. Range: 7cm, Pulse frequency: 3MHz, 1D-array, 100 element. elements size $\lambda \times \lambda$ square



3.3 Algebraic Model Estimation

The purpose of the algebraic model is to estimate the beam width from the aperture size and focal distance it is made using the data from the simulation. See Figure 3.5 for the complete work flow of the model estimation and validation process.

Figure 3.5: Block diagram of work flow for model estimation and validation



The variables are first investigated independently as seen on Figure 3.3 when the aperture is greater than 20λ the relation becomes linear. This mean the algebraic model can take the form $y = ax + b$ when all other influential variables are kept constant. For the other independent variable, negative focus, there is a decaying effect of the beam width, with longer negative focus. It approaches a constant asymptotically which seem to be equal to be the length of the aperture, see Figure 3.4. This mean the model can take the form $y = a/(-x) + b$ when all other variables are kept constant and b might be substituted with x . combining these two functions results in the Function 3.1 which can be used to determine the beam width of a negative focused array.

$$y = \frac{a \cdot x_1}{-x_2} + x_1 \quad (3.1)$$

Where x_1 is the aperture length in λ , x_2 is the negative focal distance in λ , y is the beam width in λ , and a is a constant which needs to be numerically determined.

In Formula 3.1 a will be determined by numerical optimization with a trust region algorithm and then the model will be tested against simulated data to see how well it fits.

To create the simulated data, for validation of Formula 3.1, selected intervals for the independent variables are chosen. The aperture size will span from $20\lambda=1\text{cm}$ to $50\lambda=2.5\text{cm}$ as smaller or larger arrays are rarely used. The focal distance will start at $-3\text{cm}=-60\lambda$ to $-30\text{cm}=-600\lambda$ as change in the beam width becomes neglectable when the focal distance exceeds -600λ and seem to have a singularity close to 0cm . See table 3.1 simulation 2.

Using non-linear least squares to fit the simulated data to a function and Trust-Region algorithm to numerically determine the constant a . See results in table 3.2. From this, a is recognized as being very similar to the range, $7\text{cm} = 136\lambda$ and if a

Table 3.2: Fitting result of Equation 3.1

Coefficients	a	Sum of squared error	root mean sum of squares	r^2
	137.3	976.2	1.478	0.9962

is substituted with the range (z) the Formula 3.2 is obtained. The similarity of a and the range also occurred at other ranges as seen on Figure 3.6.

$$y = \frac{z \cdot x_1}{-x_2} + x_1 = \frac{z + (-x_2)}{-x_2} \cdot x_1 \quad (3.2)$$

Where z is the range in λ . This formula is recognized to be the scaling of a triangle see Figure 3.7. The beam width estimated with Formula 3.2 can also be thought of as a projection of the aperture and is visualized in Figure 3.8 created from simulated data. When a is substituted with z the function becomes a perfect projection, and the fitting of this function needs to be reevaluated, the new fit is seen in Figure 3.9.

Figure 3.6: 6 estimations of a using ranges at 5-10cm illustrating the similarity between a and the range

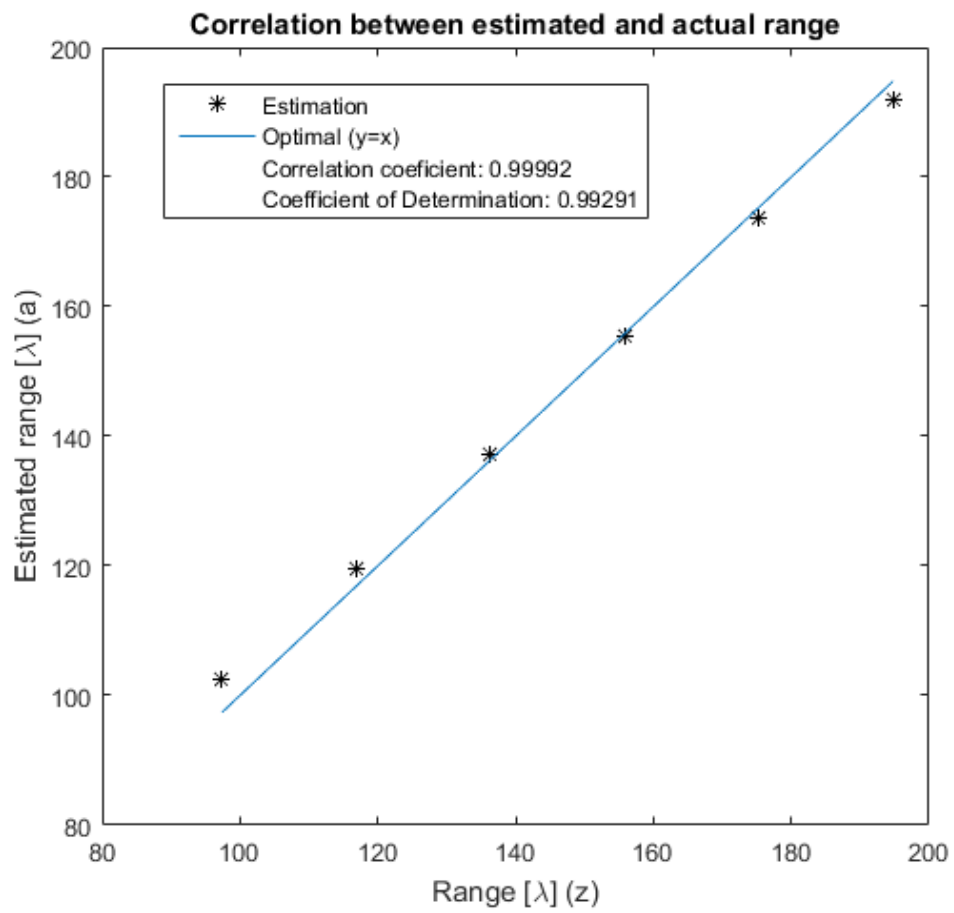


Figure 3.7: The scaling of a triangle, as recognition of the beam width is a projection of the aperture z is the range, x_1 is the aperture width also known as D , x_2 is the length from the aperture to the focus also known as F , y is the beam width

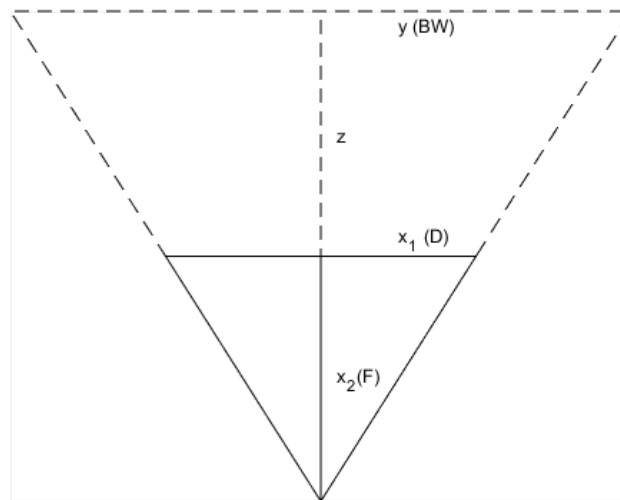


Figure 3.8: Illustration of the projection of the aperture created from simulated data.

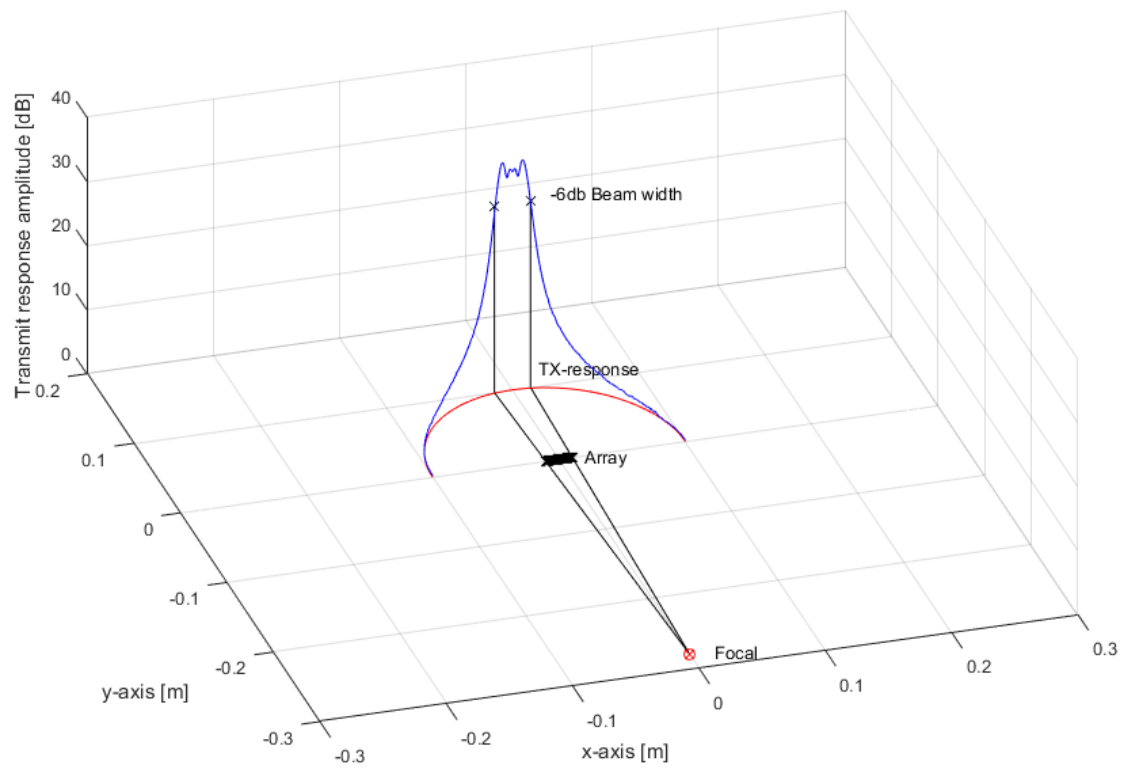
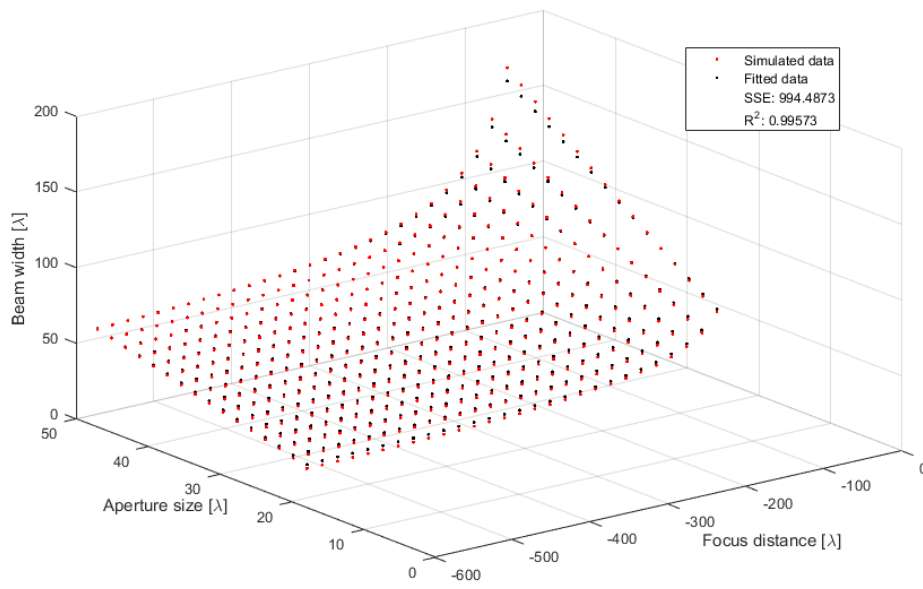


Figure 3.9: fit of triangular scaling function on simulated data

3.4 Experimental protocol

The algebraic model will be validate simply by measuring the beam width of two transducers, the VMI and S12, at two different ranges and with two different negative focus. Then the measurements will be compared with both the result of a simulation with identical setup and the result of the algebraic model. The measurements will be done in a water tank, at range 7 and 10 cm, with the frequency of the selected transducer. The focus distances will be -10 and -20 cm. This results in 8 beam width measurements composed of 41 coherent pulse measurements each. The measurements was done using a hydrophone and an oscilloscope in a water tank. See Appendix A for a description of the of the transducers and the equipment used for measuring

3.4.1 Procedure

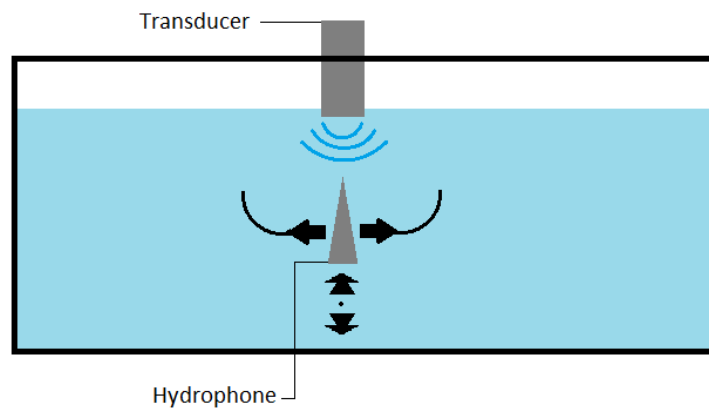
The transducer and the hydrophone are place facing towards each other in the water tank. The transducer will emit a beam. When the beam reaches the hydrophone the pressure wave will be converted to a electrical signal which is then visualized and recorded with the oscilloscope. It is important to ensure correct placement of the transducer and the hydrophone. To centralize the hydrophone in the beam a focused beam will be used. The beam will be focused at range on axis, this is done before each negative focused beam width is measurement to ensure correct positioning. The hydrophone will be adjusted for maximum peak amplitude measured with the oscilloscope. The adjustment is done in 2 dimensions of translation, in the plane parallel to the transducer, the range is adjusted with a ruler. When the correct position has been found the hydrophone will be rotated around the center of the transducer in an arc in the azimuth plane See Figure 3.10. The recording of the coherent pulse is done at each 1° of rotation from -20° to 20° , leaving 41 measurement for each beam width a total of 328 coherent pulse measurements.

In order to obtain sufficient resolution of the measurements the spacing of the measurements has to be less than the Rayleigh criterion. which has been calculated for each transducer in Equation 3.3 and 3.4.

$$vmi\theta_{max} = \sin^{-1}\left(\left(\frac{1540\frac{m}{s}}{3.57MHz}\right)/2.1cm\right) = 1.1770^\circ \quad (3.3)$$

$$s12\theta_{max} = \sin^{-1}\left(\left(\frac{1540\frac{m}{s}}{7.14MHz}\right)/9.6mm\right) = 1.2874^\circ \quad (3.4)$$

Figure 3.10: The setup for measuring the beam width of negative focused beam. The hydrophone has 3 degrees of freedom in translation and one rotational degree of freedom, in azimuth plane rotating around the center of the transducer.[4]



Chapter 4

Results

In this chapter the result of the measurements will be shown and elaborated on. For comparison the similar simulation to the measured settings has been added. For validation the algebraic model has been calculated for each of the 8 measured beam width.

As seen in Figure 4.1 to 4.8 the simulation is similar to the measured data, and as seen in table 4.1 every simulation have a correlation of at least 0.96 which is consider highly correlated this validates the simulation as a reasonable reliable way to simulated the ultrasound beam.

Table 4.1: Correlation coefficient between simulation and measured data

	S12	VMI
Z:7/F:-10	0.96538	0.97719
Z:10/F-10	0.98491	0.97682
Z:7/F:-20	0.96823	0.97041
Z:10/F:-20	0.98883	0.97316

In Figure 4.1 to 4.8 shows the similarity between the measured and the simulated CRP and the beam width for both transducers. The -6dB angles are shown on each side for both simulation and measurements. For validation of the algebraic model it has been added and the correlation coefficient between simulated and measured data has also been added. The angles of the beam widths is estimated with linear extrapolation between to two closest data point for both measured and simulated data.

Looking at table 4.2 six of the algebraic estimated beam widths are in between the simulated and measured result. In two cases were the algebraic estimated beam widths larger then both the simulated and measured beam width the two S12 transducer measurements width ranges 7cm see Figure 4.5 and 4.7. In two

Table 4.2: An overview of the full beam width results for the measured and simulated data and the corresponding output for the algebraic model for both transducers. Z is the range in cm, F is the focal distance in cm

Beam widths	S12			VMI		
	Simulated	Measured	Algebraic	Simulated	Measured	Algebraic
Z:7/F:-10	12.53 ^o	11.07 ^o	12.99 ^o	28.62 ^o	26.07 ^o	26.81 ^o
Z:10/F:-10	10.32 ^o	10.78 ^o	10.76 ^o	23.45 ^o	20.82 ^o	22.59 ^o
Z:7/F:-20	9.87 ^o	9.38 ^o	10.38 ^o	22.65 ^o	19.42 ^o	21.86 ^o
Z:10/F:-20	7.61 ^o	8.32 ^o	8.11 ^o	17.51 ^o	15.09 ^o	17.33 ^o

cases were the algebraic model smaller than the measured beam width, the two S12 measurements with ranges 10cm see Figure 4.6 and 4.8. One case were the measured beam width larger than the simulated beam width the S12 transducer with range 10cm and focus -20cm see Figure 4.8. The root mean sum of squares error (RMSE) was calculated to illustrate this similarity between the different angles. The RMSE between the simulated beam width angles and the measured beam width angles was 2.0247 and was the largest different. The RMSE between the simulated beam width angles and the algebraic beam width angles was 0.8357 and was smallest different, this was expected since the algebraic model was modeled after simulated data. The RMSE between measured beam width angles and algebraic beam width angles was 1.5565. The coefficient of correlation (CC) was calculated for the different angles. The CC between the simulated estimated angles and the measured angles was 0.9934. The CC between the simulated estimated angles and the algebraic estimated angles was 0.9996. The CC between measured angles and algebraic estimated angles was 0.9904 this shows that the results was highly correlated.

Figure 4.1: The measured and simulated Transmit response for the VMI transducer at 7cm with a focus of -10cm, with the two independent -6dB cutoff angles marked with a 'x' and the -6dB Full beam width calculated to $26.0674 \pm 0.21995^\circ (\pm 1SD)$

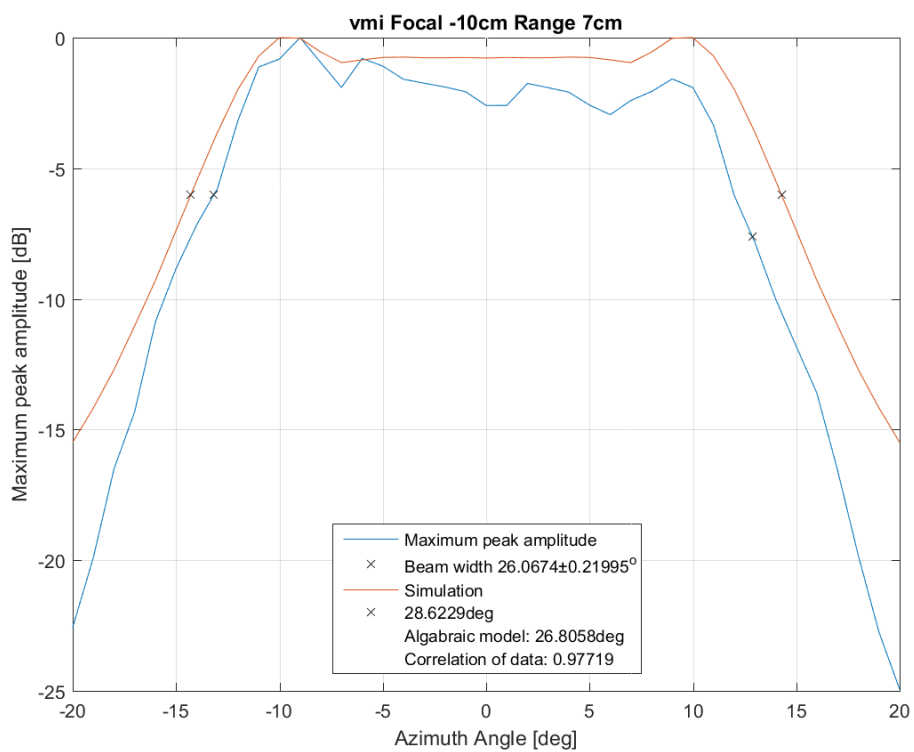


Figure 4.2: The measured and simulated Transmit response for the VMI transducer at 10cm with a focus of -10cm, with the two independent -6dB cutoff angles marked with a 'x' and the -6dB Full beam width calculated to $20.8244 \pm 0.50834^\circ (\pm 1SD)$

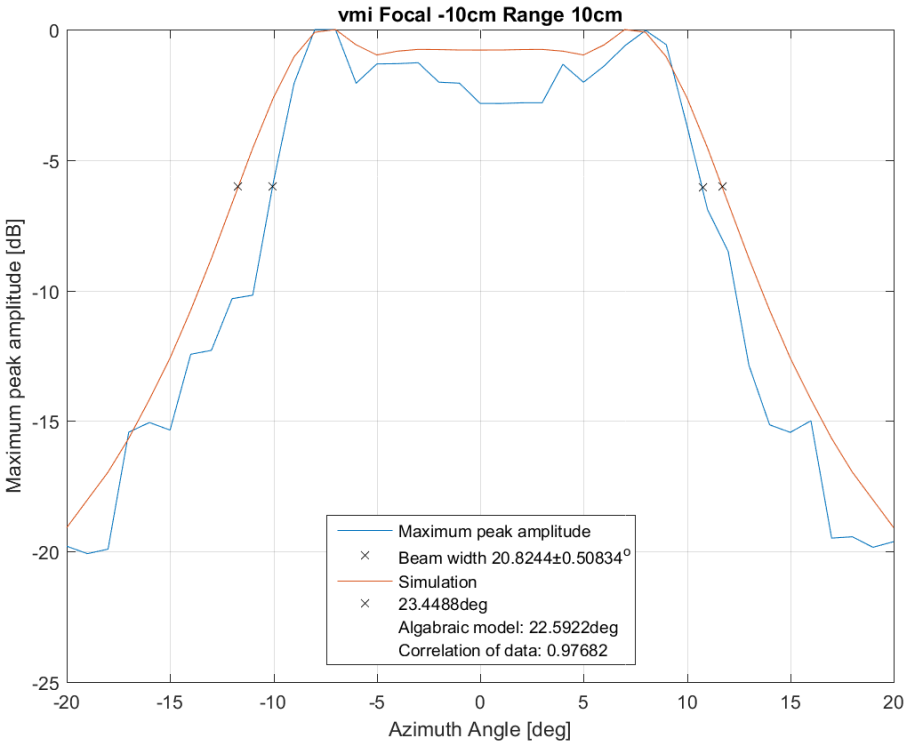


Figure 4.3: The measured and simulated Transmit response for the VMI transducer at 7cm with a focus of -20cm, with the two independent -6dB cutoff angles marked with a 'x' and the -6dB Full beam width calculated to $19.424 \pm 0.003324^\circ (\pm 1SD)$

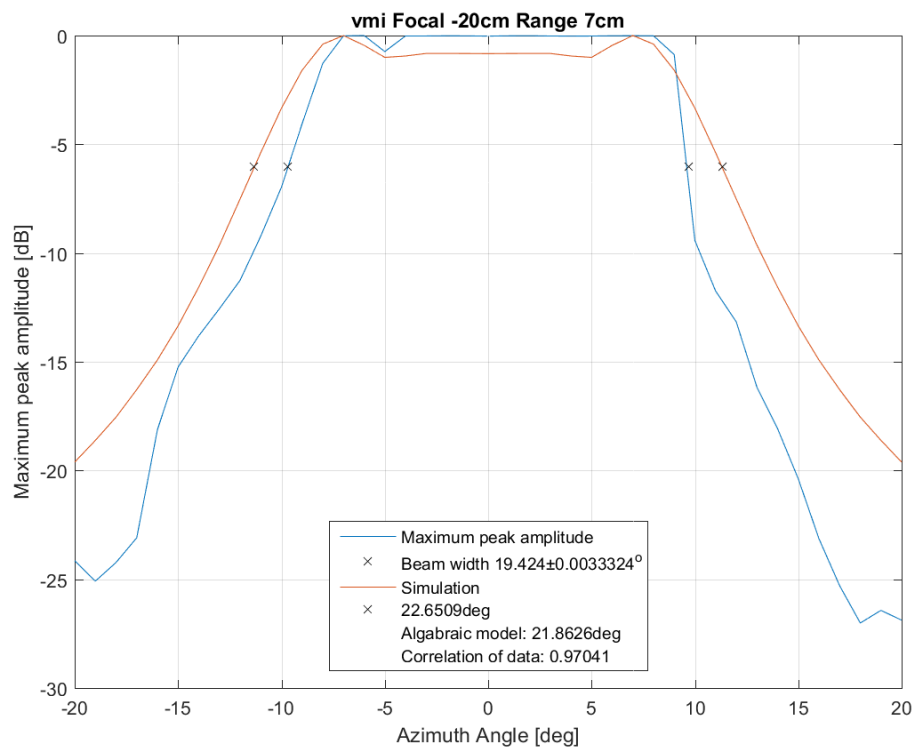


Figure 4.4: The measured and simulated Transmit response for the VMI transducer at 10cm with a focus of -20cm, with the two independent -6dB cutoff angles marked with a 'x' and the -6dB Full beam width calculated to $15.0944 \pm 0.70966^\circ (\pm 1SD)$

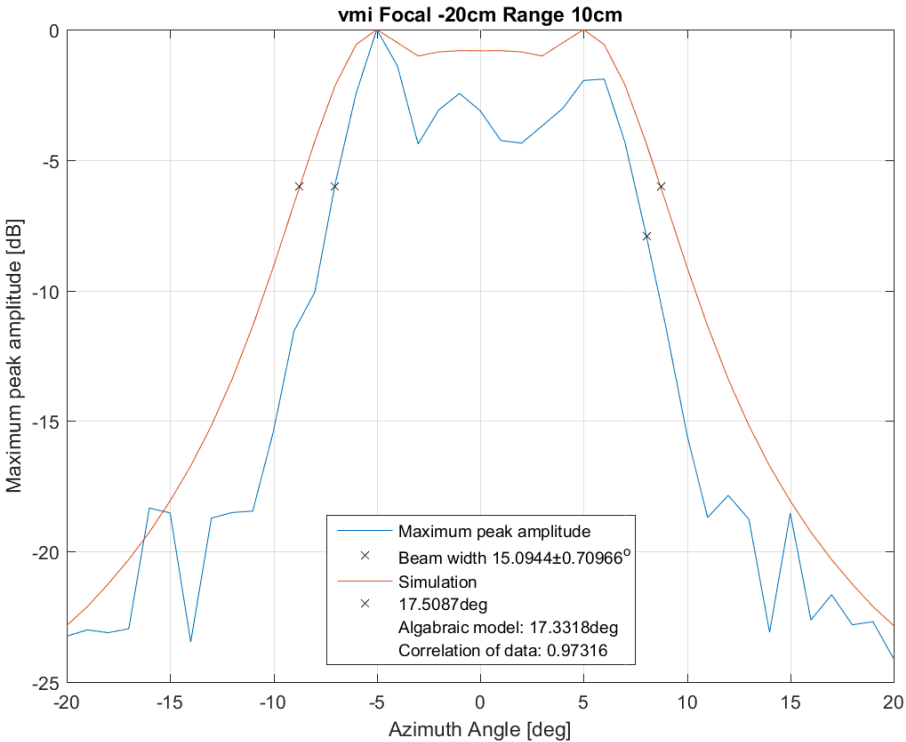


Figure 4.5: The measured and simulated Transmit response for the s12 transducer at 7cm with a focus of -10cm, with the two independent -6dB cutoff angles marked with a 'x' and the -6dB Full beam width calculated to $11.0693 \pm 0.29371^\circ (\pm 1SD)$

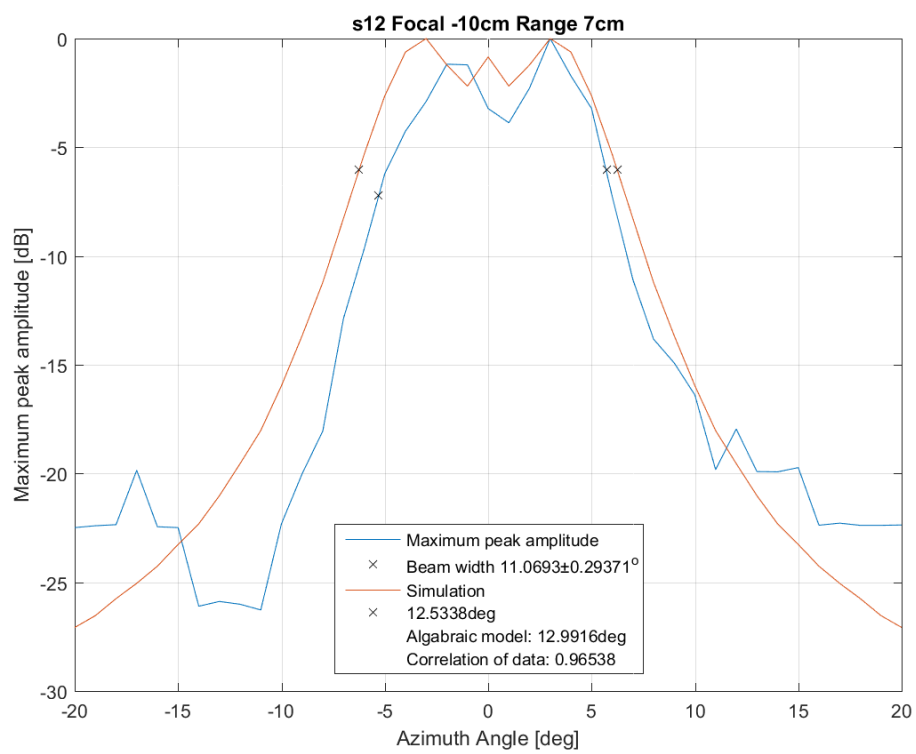


Figure 4.6: The measured and simulated Transmit response for the s12 transducer at 10cm with a focus of -10cm, with the two independent -6dB cutoff angles marked with a 'x' and the -6dB Full beam width calculated to $10.775 \pm 0.32286^\circ (\pm 1SD)$

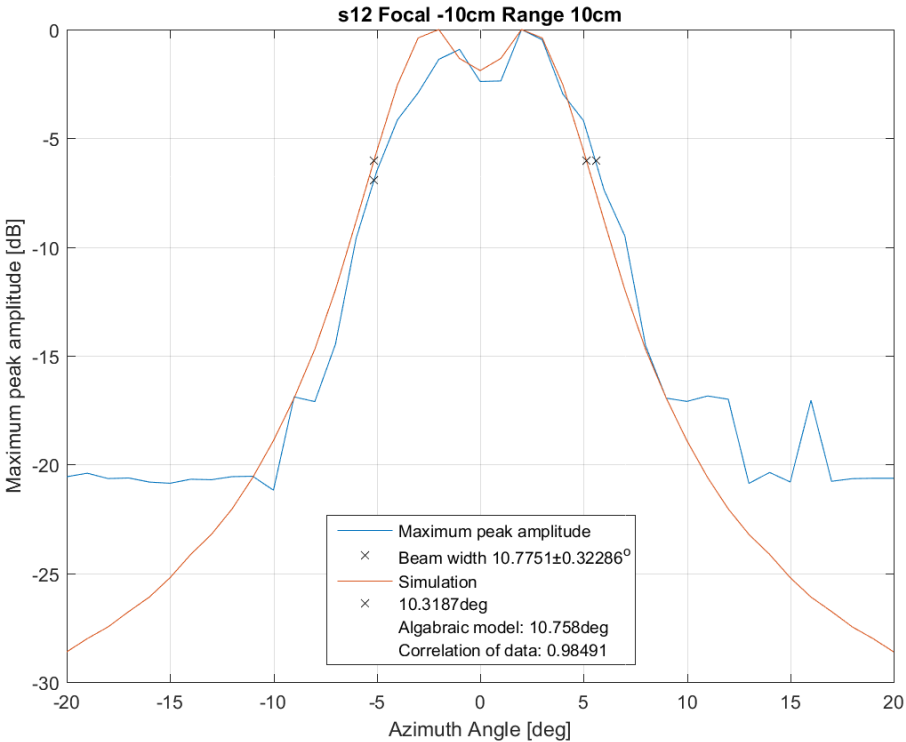


Figure 4.7: The measured and simulated Transmit response for the s12 transducer at 7cm with a focus of -20cm, with the two independent -6dB cutoff angles marked with a 'x' and the -6dB Full beam width calculated to $9.379 \pm 0.87055^\circ$ ($\pm 1SD$)

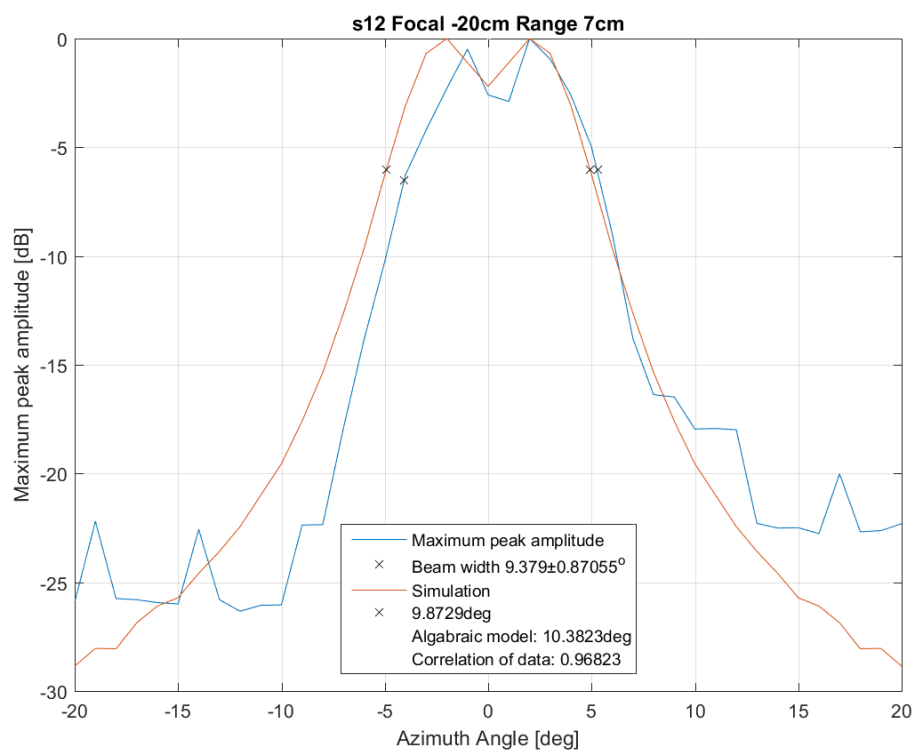
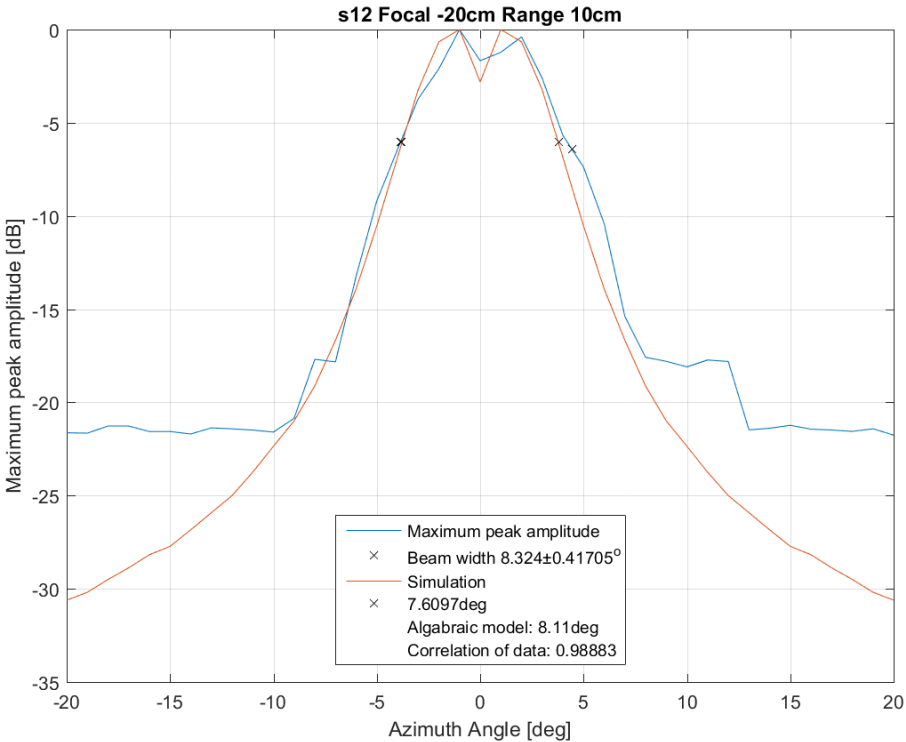


Figure 4.8: The measured and simulated Transmit response for the s12 transducer at 10cm with a focus of -20cm, with the two independent -6dB cutoff angles marked with a 'x' and the -6dB Full beam width calculated to $8.324 \pm 0.41705^\circ (\pm 1SD)$



Chapter 5

Discussion

The initial problem was created to gather the necessary knowledge and information to adequately estimate a model. First the general ultrasound was described, how it works and is applied, in order to gain a foothold in the terminology and techniques used. Afterwards it was necessary to achieve knowledge of how to simulate the different beams. The technique developed in previous work was selected and the steps from settings to coherent pulse to CRP to the beam width calculation was described. In order to go from the simulation to a model an investigation of the mathematics used to describe other beam types was necessary. Another method of simulation could have been chosen however since inaccuracies, stemming from some of the approximation, was used these were avoided. The mathematics had no directly translatable descriptions. However, it did offer direction towards the model being some geometric shape or scale with maybe a constant involved.

The method used, to get to the model, was two steps of curve fitting, one for each variable and a two dimensional for the joint function. The fitting was done with simulated data. Measured data could have been used however all influential factors would also have been modeled e.g. the bias shown in the lack of symmetry. This would not have led to a simple model and would have required hundreds of hours of measurement to obtain a similar amount of data.

The unfocused and focused beam is well described in comparison there is a lack of knowledge for the negative focused beam. Formula for determining characteristics for the other beams was found however, no description for any of the variables describing the negative focused beam was found. As parallel focusing relies on obtaining a desired beam width, the negative focused beam seems suited for this task as the beam widens with shorter negative focus. However there were no ways to determine the beam width without doing the simulation.

The mathematical knowledge obtained from the focused and unfocused case did help towards a solutions which could describe the negative focused beam but it was necessary to investigate some of the variables before a initial model could be made. A formula describing the beam width with the aperture size and negative focus distance was conceptualized with the addition of a constant (a) which was numerical determine. The constant was optimized against 448 different simulation six times with six different ranges and was recognized as the ranges. The new formula was validated with good result and thus become the algebraic model.

To interpretate the results it is important to understand the assumptions behind every different way data has been gathered. The algebraic model was created from multiple different stages of simulated data determine with a newly developed technique.

From all simulated data the beam width was calculated with no account for ripple or signal strength. This put some constraints on the capability of the model. As an example the model would allow to pick the focal distance for any existing aperture to obtain a desired beam width. However, will not describe if the beam has an usable ripple or enough energy to generated a detectable echo. The relationship between beam width, ripple and signal strength still remain uncertain however, it is possible to state that a wider beam reduces signal and increases ripple.

In Figure 4.1 to 4.8 it is seen that the ripple is approximately 1-4 dB. This is within an acceptable range. The ripple could be influential on the beam width calculation, as there are different ways to determine the -6 dB cutoff, where the ripple is a major factor. Instead of using the maximum peak value as reference, the center value or the average value between the peaks could have been used which would change the beam width. Using one of these two other options as reference points for the -6db cutoff would decrease the value and thus the cutoff would move down the slope. An effect resulting in a wider beam and since the model predicts a wider beams than in the measurement in the majority of the data this would not improve the accuracy of the prediction.

The results show the simulated beam width to be larger than the measured beam width in all cases with the VMI transducer. The algebraic model did better than the simulated model but was still closer to the simulated beam widths than the measured beam widths. However the simulated and algebraic results should not be completely disregarded for this bias. The measured data have some bias itself, most noticeable is the lack of symmetry which is a confirmation of the bias influencing the measurements reducing the precision. The influence of the hydrophone might attenuated some elements more than others due to the angle of acceptance reducing accuracy.

The algebraic model was determined from simulated data where in cases of very small aperture did not behave linear see Figure 3.3. The algebraic model only depict the linear part but an description of the nonlinear part might be the elements overlapping resulting in a similar effect as mechanical coupling between the element which mean they appear larger than they are, inhibiting the beam spread at first. As the overlap grows when the aperture get smaller, the aperture begins to behave as a single element making the beam more and more similar to the directivity function, which in this case of a $\lambda \times \lambda$ element is spherical.

The algebraic model also makes some interesting predictions about the positive focus, and unfocused beam. The unfocused beam can be consider as placing the focus at plus or minus infinity which reduces the formula so the beam width is equal to the aperture size which correspond with the behavior of the unfocused beam. The positive focus predicts when $Z = F$ the terms cancel out and the beam width becomes zero this is in practice impossible but does depict the very narrow beam of the Tx response when in focus.

As stated the negative focused beam has a unknown relationship where the beam could be considered to be split in two when the negative focus gets close to the aperture it is hypothesized that it is around $F < D/2$ which results in a beam width larger than 90° which is more than the common practice field of view. It can be hard to find an area of application of the negative focused beam since some of the problems in ultrasound transducer design arise from the limited signal strength and then why would anyone spread the signal even thinner, however this model provides tools to optimize the beam width to match any improvement in sensitivity of a transducer gaining more information pr. Tx-Rx cycle thus giving the opportunity to increase frame rate.

Chapter 6

Conclusion

Problem statement: *How does the aperture size and focal distance influence the beam width of an negatively focus transmit response?*

The beam width becomes a projection of the aperture thus a bigger aperture results in a bigger beam width. The negative focus reduces the beam width with longer distance however, cannot reduce it below the size of the aperture.

$$B\hat{W} = \frac{\hat{Z} \cdot \hat{D}}{-\hat{f}} + \hat{D} = \frac{\hat{Z} - \hat{f}}{-\hat{f}} \cdot \hat{D} \quad (6.1)$$

The final Formula 6.1 for the algebraic model, $B\hat{W}$ is the beam width in wavelength, \hat{Z} is the range in wavelength, \hat{f} is the focus distance in wavelength \hat{D} is the aperture size in wavelength. The algebraic model makes a adequate prediction of the negative focused beam width however does not take to account of signal or ripple. it does not work for larger element, where the individual element is not considered a spherical source, and is only tested on 1D array.

Them model provides an easy geometric way of understanding the fundamental shape of the beam. With further research the model has the potential to include the unfocused and positive focused beams as well. This could potentially create a combine theory of the beam functions thus reducing the complexity of the field and make it easier for advancement. For a detailed depiction of a given scenario the entire simulation must be acquired and studied. At this time the model make it easier to assess some of the variables before the simulation and thus having more control of the outcome.

Bibliography

- [1] John E Aldrich. “Basic physics of ultrasound imaging”. In: *Critical care medicine* 35.5 (2007), S131–S137.
- [2] Haim Azhari. *Basics of biomedical ultrasound for engineers*. John Wiley & Sons, 2010.
- [3] John Maxwell Cowley. *Diffraction physics*. Elsevier, 1995.
- [4] Christian Elmholt Jakobsen. *Generic Ultrasound transducer simulation*. http://projekter.aau.dk/projekter/files/225234872/Generic_Ultrasound_transducer_simulation.pdf. 2015.
- [5] Cooper Moore et al. “Live high-frame-rate echocardiography”. In: *Ultrasonics, Ferroelectrics, and Frequency Control, IEEE Transactions on* 62.10 (2015), pp. 1779–1787.
- [6] ONDA. *HGL Hydrophones*. http://www.ondacorp.com/images/brochures/Onda_HGL_DataSheet.pdf. 2015.
- [7] Thomas L Szabo. *Diagnostic ultrasound imaging: inside out*. Academic Press, 2014.
- [8] Agilent Technologies. *Agilent 6000 Series Oscilloscope*. <http://cp.literature.agilent.com/litweb/pdf/54684-97011.pdf>. 2006.
- [9] Olaf T Von Ramm and Stephen W Smith. “Beam steering with linear arrays”. In: *Biomedical Engineering, IEEE Transactions on* 8 (1983), pp. 438–452.
- [10] Shi-Chang Wooh and Yijun Shi. “Three-dimensional beam directivity of phase-steered ultrasound”. In: *The Journal of the Acoustical Society of America* 105.6 (1999), pp. 3275–3282.

Appendix A

Equipment

A.0.1 Hydrophone

Each measurement will be done with the OndaCorp HGL-0200 Hydrophone. The hydrophone catches the acoustics energy emitted from the transducer and converts it to an electric signal which the oscilloscope can record. The -6db band width of the hydrophone is 0.25MHz to 40Mhz and the angle of acceptance is 100° , which is the angle between the two mirroring points where signal is attenuated -6db. The hydrophone is also equip with a 20db pre-amplifier.see Appendix B for more information on the hydrophone.[6]

A.0.2 Oscilloscope

The Agilent DSO6034A oscilloscope has 4 channel two of which is used in the setup. One channel for the pulse trigger and the other to measure the signal from the hydrophone. The oscilloscope is capable of 2GSa/s and has a bandwidth of 300MHz [8]

A.0.3 VMI transducer

Is a 3.57MHz transducer with an 1 dimensionally array that measures 21mm in width and 14mm in height. It consist of 96 element each with a width of $220\mu m$ all data of this custom transducer was provided by Duke University Biomedical department.

A.0.4 HPS 12 transducer

Is a 7.14Mhz transducer with a 1 dimensionally array that measures 9.6mm in width and 7mm in height. It consist of 96 element each with a width of $100\mu m$ all data of this commercial transducer was provided by Duke University Biomedical department.

Appendix B

Hydrophone datasheet

HGL Hydrophones

The HGL Series hydrophones were designed to meet or exceed recommendations of section 3.3.2 of the AIUM Acoustic Output Measurement Standard (May 1998). They have an exceptionally flat sensitivity in a small and sturdy package. These hydrophones are excellent in-house standards for ultrasonic acoustic intensity measurements, and for general purpose field mapping.

Features

- High sensitivity
- Small effective aperture
- Broadband
- Solid construction
- Flawless integration with AH preamplifiers
- Flat (+/-3dB) 250 KHz to >> 20 MHz *

* Use of the AG-20X0 preamplifier is required to maintain +/- 3 dB range from 20 to 40 MHz for the HGL-0085 and HGL-0200. For measurements above 40 MHz, the AH-20X0 preamplifier is advised.

Technical Specifications

	HGL-0085	HGL-0200	HGL-0400	HGL-1000
Frequency range ($\pm 3\text{dB}$)	0.25 to 40 MHz		0.25 to 20 MHz	
Electrode aperture	85 μm	200 μm	400 μm	1000 μm
* EOC Nominal Sensitivity [dB re 1V/μPa]	-278	-266	-251	-240
* EOC Nominal Sensitivity [nV/Pa]	13	50	282	1000
Acceptance angle (-6dB at 5 MHz)	>150°	100°	30°	20°
Capacitance	30 pF			
Max. Operating Temperature	50 °C			

* EOC ("end of cable") is the open-circuit output sensitivity of the hydrophone. Calibration with an amplifier can be determined from the gain and input impedance of the amplifier.

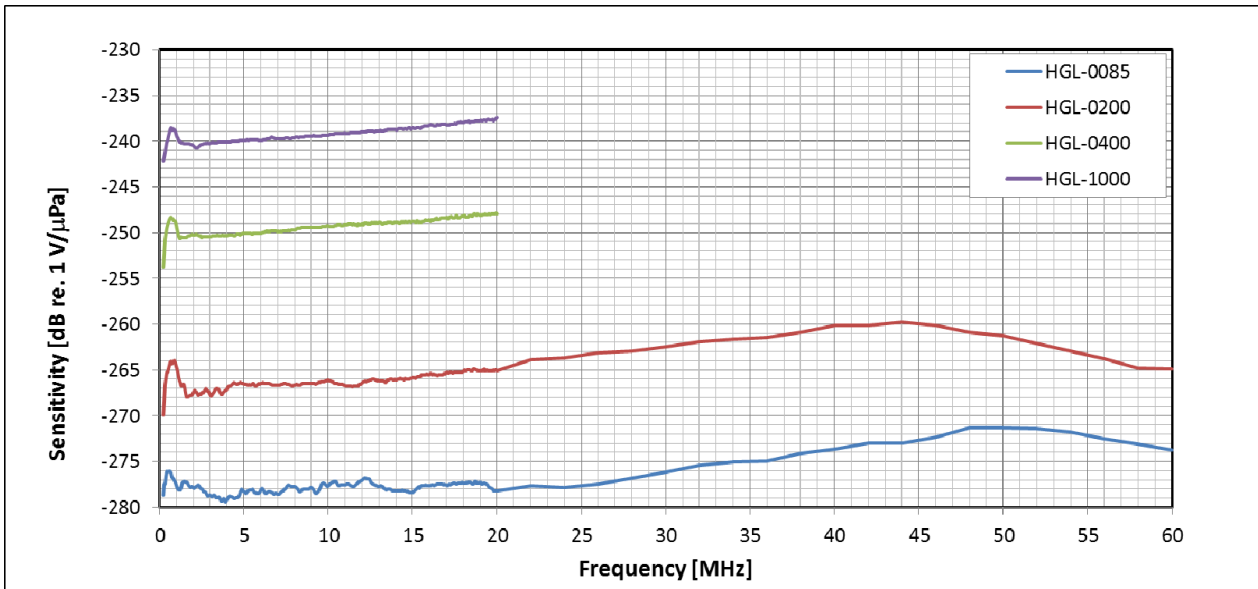
Provided with traceable calibration 1-20 MHz at 50 KHz intervals. For other calibrations available visit our web site.

Specifications are subject to change without notice.

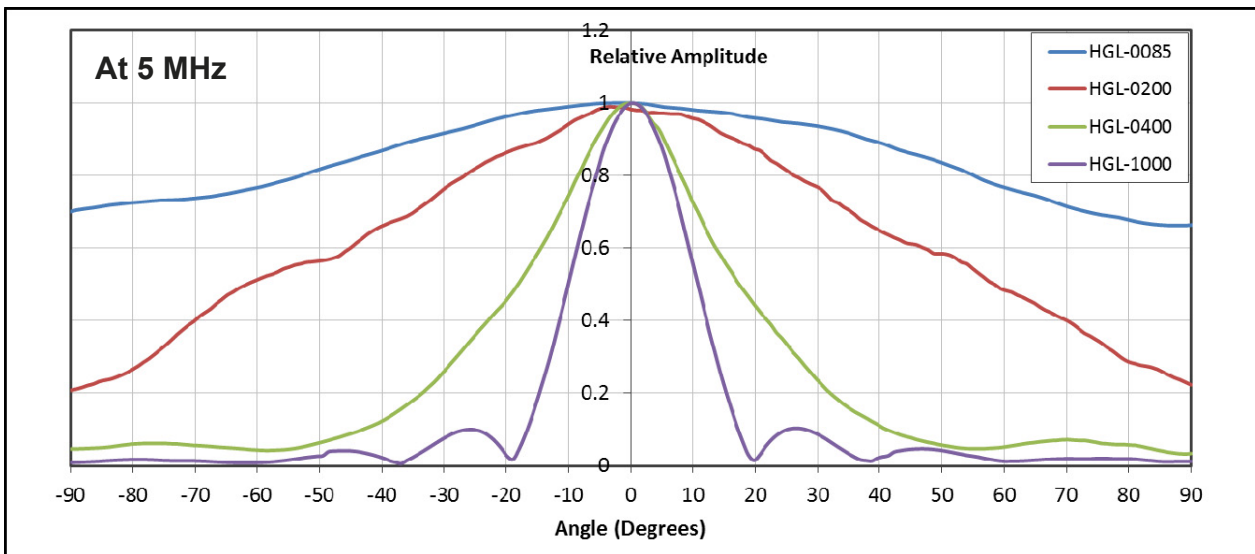


HGL Hydrophone

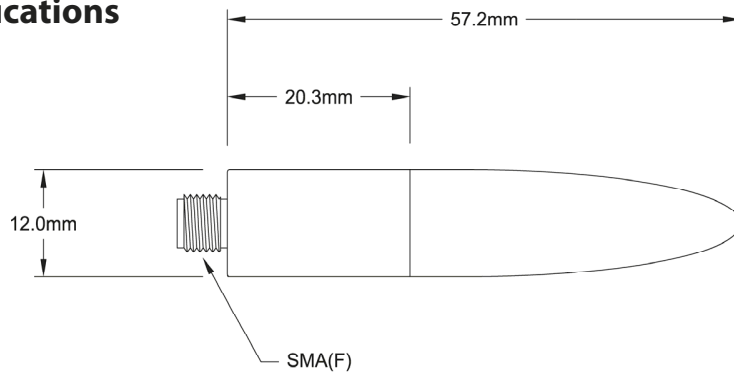
Typical Sensitivity Plot



Typical Directivity Plots



Mechanical Specifications



Appendix C

Model formulation

This Appendix is a copy of the model formulation from my previous work, form 9. semester. It describe how the method, created to simulate beam plots works and how the different parts are calculated

This Chapter will mainly focus on how the mathematics of the physics is applied in the software solution. The necessary information of how it works and why the choosen concepts is important is presented in the problem analysis. the conceptualization will focus on how to apply the formulas and how the different concepts interfere however will only be describe on a mathematical level with limited explanation of programming since it is too extensive to cover completely. The Realization will focus on how the simulation is presented and what tools is necessary to make a meaningful interpretation of the simulation. The solution section will be a presentation of the final prototype of the software and how the GUI works. The Validation section will compare simulations with measured data collected trough experiment also explained within this section.

C.1 Conceptualization

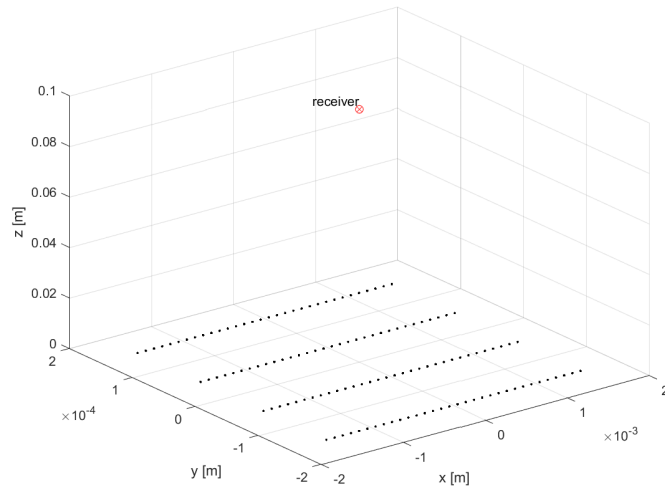
From the previous chapter the ultrasound simulation can be divide into two parts. the first is the accurate summation of the coherent pulse, second is use and display of the data gathered from the different coherent pulses these two part will be presented in this Section and Section C.3. The calculation of the coherent pulse require knowledge of each pulse origin, amplitude and distance to the point, where the coherent pulse is measured (the receiver).

C.1.1 Coherent Pulse

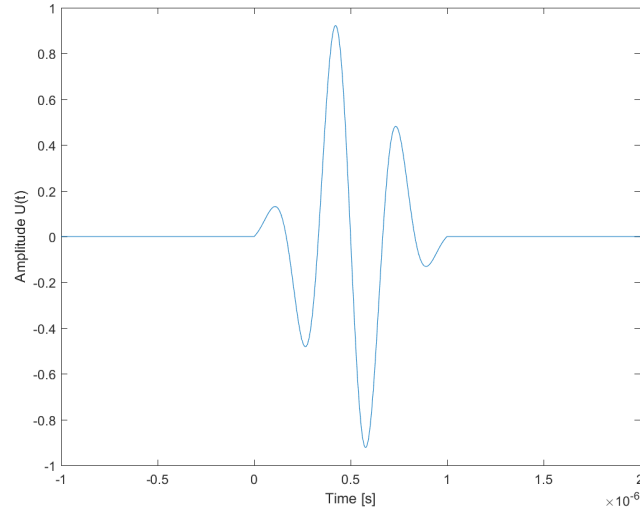
The variation of the coherent pulse amplitude depend on both the element energy conversion rate and transmit voltage. The simple solution is to give it amplitude of a mathematical unit of 1-peak-amplitude. If the amplitude of each pulse is the same at emission, then end result can be scaled accordingly after summation. The origin of the pulse is the center of an element. the elements can be arrange in many patterns therefore it is important to know where they are located. Each element center can be represented with 3 cartesian coordinates in a 3-dimensional euclidean space for all settings see Figure C.1. likewise can the receiver be represented this way, but since information is gathered and beam is steered using polar or ballistic coordinates this notation is chosen. polar or ballistic coordinates makes it simple to visualize the receivers placement and can converted to cartesian coordinates when the distance between each element and the reciever (d_i) is calculated using Pythagoras theorem.

The pulse is best represented in a time-amplitude function as $U(t, P_f, P_d)$ where t is the time, P_f is the pulse frequency and P_d is the pulse duration. The pulse function is a sinusoid overlayed by a gaussian function and a rectangular window function. P_f and P_d will remain constant for an entire simulation and thus the pulse function will be refer to as $U(t)$ see Figure C.2 and Equation C.1.

Figure C.1: Center of elements in a array 32 by 4 with a distance of 0.1mm represented in eucleadean space. Receiver place with $\theta = 0^\circ$ and $\phi = 0^\circ$ at a distance of 10cm.



$$U(t) = \begin{cases} \sin(P_f \cdot x) \cdot \text{gausswin} & 0 \leq x \leq P_d \\ 0 & \text{Otherwise} \end{cases} \quad (\text{C.1})$$

Figure C.2: pulse function with a frequency of 3MHz and a duration of $1\mu\text{s}$ 

The pulses will likely arrive at different time to the receiver the individual pulses might be considered as $U(t - d_i/c)$ where c is the speed of the pulse (1540 m/s speed of sound in tissue). Then the coherent pulse $U_z(t)$ may be calculated as seen in Equation C.2 where N is the number of elements and seen as an example in Figure C.3

$$U_z(t) = \sum_{i=1}^N U(t - \frac{d_i}{c}) \quad (\text{C.2})$$

C.1.2 Time delay

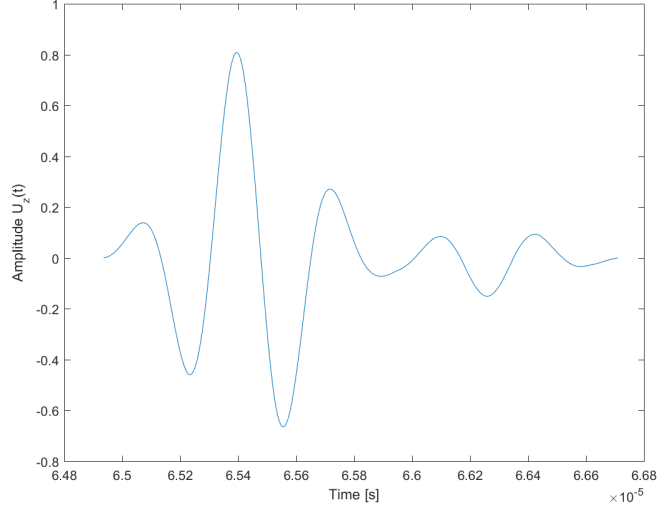
The phased array uses small delays for each element to steer and focus the wavefront which in time make up the beam. This is implemented as t_i in Equation C.3 where it delays the pulse and shift their timing e.g. to match each pulse in phase in the focus point. see Section ?? and ?? for examples and calculation of different time delays.

$$U_z(t) = \sum_{i=1}^N U(t - \frac{d_i}{c} + t_i) \quad (\text{C.3})$$

C.1.3 Attenuation

All Attenuation affects the individual pulses differently since the distance and angle to the receiver differs between elements. The frequency dependent attenuation

Figure C.3: plot of coherent pulse function at 3MHz and a duration of $1\mu s$, 32 elements in a single line 1mm apart. receiver is at distance of 100mm at $\theta = 0$ and $\phi = 0$



is also dependent on the range and thus each attenuation has to be applied to the individual pulses before summarizing them to the coherent pulse see Equation C.4

$$U_z(t) = \sum_{i=1}^N U\left(t - \frac{d_i}{c} + t_i\right) \cdot A_f(f, d_i) \cdot A_d(d_i) \cdot A_{angle}(\theta_i, \phi_i) \quad (C.4)$$

where $A_f(f, d_i)$ is the frequency dependent attenuation, $A_d(d_i)$ is range dependent attenuation, $A_{angle}(\theta_i, \phi_i)$ is the angle dependent attenuation.

C.2 Attenuation due to frequency

The attenuation coefficient is normally given as $\alpha = \frac{dB}{cm \cdot MHz}$. To find the attenuation in dB at the traveling distance and frequency must be known and multiplied, $dB = \alpha \cdot d_i \cdot Pf$ and then transform from dB to gain see Equation C.5.

$$gain = 10^{\frac{dB}{20}} \Rightarrow gain = A_f(f, d_i) = 10^{\frac{\alpha \cdot d_i \cdot Pf}{20}} \quad (C.5)$$

C.2.1 Dissipation of the pulse (Attenuation due to range)

As determined in subsection ?? the $1/r$ had a singularity problem and thus $A_d(d_i) = \frac{k}{r+k}$ was established to circumvent that problem. A new problem arise with the determination of the constant k which will be estimated using data from measurement of a single element at different ranges. The single element pulse data showed

a drop in voltage from the hydrophone from 0.0356V at 1 cm to a 0.0128V at 5 cm which give k a value of 1.25cm see Equations C.6

$$\begin{aligned} \frac{A_d(0.05)}{A_d(0.01)} &= \frac{0.0128}{0.0356} = 0.36 \\ &\Downarrow \\ \frac{\frac{k}{0.05+k}}{\frac{k}{0.01+k}} &= 0.36 \\ &\Downarrow \\ k &= 0.0125 \end{aligned} \quad (C.6)$$

C.2.2 Directivity function (Attenuation due to angle)

The angle attenuation is influenced by many variables such as element height and width (α and L) and azimuth angle and rotational angle (for the general equation) however our input must be ballistic coordinates so an conversion from ballistic to spherical coordinates must take place first using Equation C.7 and C.8

$$\theta_S = \tan^{-1}\left(\frac{\sqrt{r \cdot \cos(\phi) \cdot \sin(\theta_B)^2 + (r \cdot \sin(\phi))^2}}{\cos(\phi) \cdot \cos(\theta_B)}\right) \quad (C.7)$$

$$\psi = \tan^{-1}\left(\frac{\sin(\phi)}{\cos(\phi) \cdot \sin(\theta_B)}\right) \quad (C.8)$$

where θ_S is the azimuth angle for spherical coordinates ψ is the rotational angle for spherical coordinates θ_B is the azimuth angle for ballistic coordinates ϕ is the elevation angle for ballistic coordinates.

C.3 Realization

The main purpose of this simulation toolbox is to give an accurate answer to the behavior of any transducer, in other terms make the necessary calculations and provide tools to pick and view different aspect of the simulation. This means that the user needs to provide all information about the transducer, pulses and timing to makes the simulation and then provide details of which information the user is interested in such as angles, range and time. The rest should be handled by the software which after the calculation should present all data requested. To investigate the data the software should be restricted to a one click approach to make it as intuitively as possible.

One of the interesting informations to find from a transducer is the maximum pulse amplitude passing through a given point in space or an overall idea of the maximum amplitude for all point in a certain area. Because it provides information

about where the echos could originating. The most used term for these maps are the beamplot which comes in many formats, such as contours, surfacesplots and images with different colormaps. This simulation will use grayscale images with a colorbar to represent max and min values. This is chosen due to the data structure and that 2D images is deem adequate to represent the data.

C.3.1 Maximum Peak Amplitude - Mapping

In the Maximum Peak Amplitude (MPA) map type the pixel value correspond to the max value of a coherent pulse. Finding The maximum of the Coherent pulse is a optimization problem. Since the pulse has multiple locale maxima See Figure C.3 the usual algorithmes such as 'Steepest accent', 'golden section search' or 'parabolic interpolation' will not be as effective, the only way to be sure to find the maximum is to use the brute force approach. The time step must be short enough that it does not conflict with the Nyquist theorem for the pulse frequency. This mean for $3Mhz$ the step size must be less then Equation C.9. The only question now is where to start and to stop the maximum search this is ultimately up to the user. However a long interval will greatly increase computation time, and the software should never start calculating the amplitude before the first pulse of the nearest element has arrived. The interval should always start when the first pulse arrives at the point of interest or later. normally the peak amplitude occurs $1-3 \mu s$ after first arrival thus having a interval of $20 \mu s$ would be extreme since that would infer the difference in distance of closest and furthest element is more then 3cm and normally a scanner would not expect and echo from a location that long. However These can be adjustable for any extraordinary circumstances in the software. On axis plot and constant range plot has proven useful when analyzing The potential of a transducer. the ability to view or extract different graphs. ether a graph of amplitude at the different ranges in a fixed angle or a graph of amplitude at a certain fixed distance at different angles. The infomation for theses two types of plots can be extracted from a MPA simulation, see Figure C.5.

$$\frac{1}{2 \cdot P_f} = \frac{1}{2 \cdot 3 \cdot 10^6 Hz} = 167ns \quad (C.9)$$

Figure C.4: Eksample of MPA mapping with: 32 element, 1D, 0.1mm apart size: 0.1mm x 0.1mm, azimuth angle: -90° to 90° , MPAstep:0:0.01:1.1 μ s, range: 0-10cm, no elevation, pulse: 1 μ s 3Mhz, no time delays

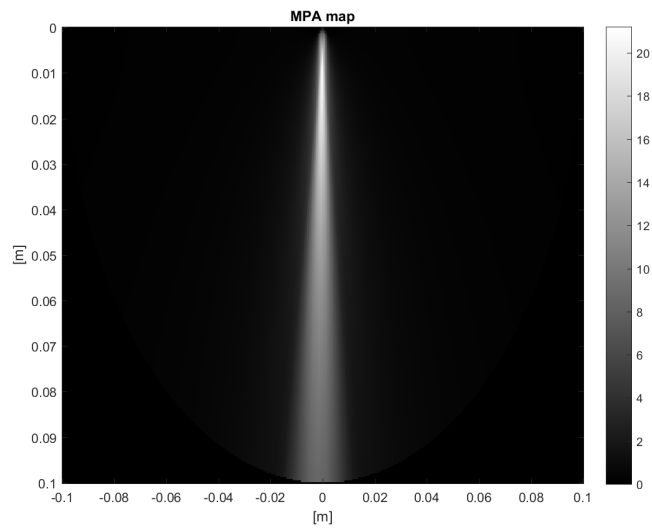


Figure C.5: A: The same simulation as in Figure C.4 with the amplitudes at 7.8cm marked in green and amplitudes at $\theta = 0^\circ$ marked in megenta. B: The angle graph shows the amplitude for all angles at a specific distance in this case 7.8cm C: The line graph shows the amplitude for all distances at a specific angle in this case 0° .

